Cancer Letters 639 (2026) 218209

Contents lists available at ScienceDirect

Cancer Letters

journal homepage: www.elsevier.com/locate/canlet

Original Articles

Lactic acid promotes an MDSC-like phenotype via HIF1α stabilization with impact on prognosis in renal cell carcinoma

Nathalie Babl [a,b,*], Florian Voll [a,b], Agnieszka Martowicz [c], Christina Bruss [a], Marianna Maddaloni [b], Christian Schmidl [b], Michael Rehli [a,b], Stefan Loipfinger [b], Nicholas Strieder [b], Claudia Gebhard [b], Petra Hoffmann [a,b], Sukh M. Singh [d], Ada Sala-Hojman [e], Roberta Ferretti [f], Carina Matos [a,b], Malte Simon [b,g], Christina Brummer [a], Annette Schnell [a], Joshua Hofbauer [a], Sonja-Maria Decking [a,b,h], Peter Hau [i], Arabel Vollmann-Zwerenz [i], Katja Dettmer [j], Peter J. Oefner [j], Michael Althammer [a], Johanna Laufs [a], Sarah Friedl [a], Timo Heinrich [e], Christian Herhaus [e], Katja Evert [k], Roman Mayr [l], Julieta Afonso [m,n], Fatima Baltazar [m,n], Wolfgang Herr [a], Peter J. Siska [a,1], Kathrin Renner [a,h,1], Marina Kreutz [a,b,**]

[a] Department of Internal Medicine III, University Hospital Regensburg, Regensburg, Germany
[b] Leibniz Institute for Immunotherapy (LIT), Regensburg, Germany
[c] Department of Internal Medicine V, Haematology & Oncology, Comprehensive Cancer Center Innsbruck (CCCI) and Tyrolean Cancer Research Institute (TKFI), Medical University of Innsbruck, Innsbruck, Austria
[d] School of Biotechnology, Institute of Science, Banaras Hindu University, Varanasi, Uttar Pradesh, India
[e] Merck Healthcare KGaA, Darmstadt, Germany
[f] EMD Serono Research & Development Institute, Inc., Billerica, MA, USA, an affiliate of Merck KGaA
[g] Division of Applied Bioinformatics, German Cancer Research Center (DKFZ), 69120 Heidelberg, Germany
[h] Department of Otorhinolaryngology, University Hospital Regensburg, Regensburg, Germany
[i] Department of Neurology and Wilhelm Sander-NeuroOncology Unit, University Hospital Regensburg, Regensburg, Germany
[j] Institute of Functional Genomics, University of Regensburg, Regensburg, Germany
[k] Institute of Pathology, University of Regensburg, Regensburg, Germany
[l] Department of Urology, Caritas St. Josef Medical Centre, University of Regensburg, Regensburg, Germany
[m] Life and Health Sciences Research Institute (ICVS), School of Medicine, University of Minho, Campus of Gualtar, 4710-057, Braga, Portugal
[n] 2ICVS/3B's-PT Government Associate Laboratory, Braga/Guimarães, Portugal

ARTICLE INFO

Keywords:
Renal cell carcinoma (RCC)
Lactate metabolism
IL-6 signaling
Myeloid-derived suppressor cells (MDSCs)
Tumor microenvironment
Tumor glycolysis
Tumor-associated myeloid cells

ABSTRACT

Paradoxically, immune cell infiltration correlates with worse prognosis in renal cell carcinoma (RCC) patients, with tumor-associated myeloid cells playing a key role in tumor progression. However, little is known about factors driving their polarization. Here, we investigated the link between RCC-related glycolysis, hypoxia-inducible factor (HIF)1α-associated myeloid inflammation, and patient prognosis.

TCGA data revealed a strong correlation between the expression of monocarboxylate transporter 4 (MCT4), the myeloid marker CD14 and patient survival in ccRCC patients. scRNAseq data confirmed high MCT4 expression in both tumor and myeloid cells, suggesting lactate transport. *In vitro* analyses proved lactate uptake by $CD14^+$ monocytes, which stabilized HIF1α and induced an MDSC-like, HLA-DR low phenotype. In line, the HIF1α-stabilizing drug Roxadustat increased the number of $CD14^+$ HLA-DR low cells. Lactate uptake also increased protein lactylation.

To further investigate the interplay between RCC tumor and myeloid cells, we established a 3D spheroid co-culture model and analyzed the effects of MCT inhibitors. This 3D model reflected tumor-myeloid cell

* Corresponding author. University Hospital Regensburg Franz-Josef-Strauß-Allee 11, 93053, Regensburg, Germany.
** Corresponding author. University Hospital Regensburg Franz-Josef-Strauß-Allee 11, 93053, Regensburg, Germany.
E-mail addresses: nathalie.babl@ukr.de (N. Babl), marina.kreutz@ukr.de (M. Kreutz).
[1] These authors contributed equally.

https://doi.org/10.1016/j.canlet.2025.218209
Received 18 November 2025; Received in revised form 3 December 2025; Accepted 6 December 2025
Available online 8 December 2025

interactions, as spheroid-infiltrating myeloid cells exhibited spontaneous IL-6 secretion comparable to patient-derived RCC cultures. Inhibition of lactate secretion reduced lactate and IL-6 secretion while increasing $CD14^+$ $HLA\text{-}DR^+$ cells. These findings were validated in patient-derived RCC cultures treated with anti-glycolytic drugs.

Our data dissect the intratumoral network of RCC and show that tumor-derived lactate promotes a pro-tumorigenic myeloid phenotype with low MHC-II but high immune-checkpoint, LOX-1 and S100A8/9 expression. Blocking MCT disrupts this interplay, offering a promising strategy to re-educate tumor-associated myeloid cells and enhance tumor immune surveillance.

1. Introduction

Renal cell carcinoma (RCC) accounts for 2–3 % of solid tumors in adults and comprises several subtypes, with the clear-cell subtype (ccRCC) being responsible for the majority of cancer-related deaths [1–4]. ccRCC is characterized by various genetic abnormalities, which lead to loss of function of the tumor suppressor gene von Hippel-Lindau (VHL). Inactivation of VHL stabilizes HIF1, which binds to regulatory hypoxia-responsive elements in DNA [5]. Subsequently, expression of more than 70 genes is induced, including *VEGF, GLUT1*, lactate dehydrogenase A (*LDHA*), and monocarboxylate transporter 4 (MCT4, *SLC16A3*) [6,7], reflecting the highly glycolytic phenotype of this tumor entity.

Overexpression of MCT4 has been described in several cancers [8,9] and analysis of TCGA data revealed a correlation between high MCT1 and MCT4 expression and poor outcome in ccRCC [3,10,11]. In line, Kim et al. described overexpression of MCT1, MCT4 and the respective chaperone CD147 as predictors of tumor progression in ccRCC [11]. Besides MCT expression, an enriched glycolysis-related signature is associated with worse RCC prognosis, and it impacts the intratumoral immune cell composition [12].

Apart from tumor cells, tumor-associated macrophages (TAMs) may contribute to lactic acidosis in the tumor environment (TME) [13]. Reinfeld et al. demonstrated that $CD11b^+$ myeloid cells isolated from murine MC38 tumors showed a high capacity for fluorodeoxyglucose (FDG) uptake [14]. In line, TAMs express LDHA [15], and myeloid-specific deletion of LDHA supported T cell anti-tumor response and reduced tumor growth [16]. Moreover, it has been shown that LDHB in TAMs is downregulated in murine and human breast cancer, thereby increasing aerobic glycolysis [17]. These data suggest that targeting the metabolism of TAMs might be an interesting option to overcome an immunosuppressive TME, besides targeting tumor metabolism.

On the other hand, myeloid cells are imprinted by lactate accumulation in the TME. Glycolytic murine tumors such as B16 melanoma and LLC lung carcinoma fostered immunosuppressive murine macrophage polarization via HIF1α stabilization [18,19]. In line with the general role of lactate in immune regulation, Sangsuwan et al. [20] showed that sodium lactate induces immunosuppressive phenotypes in murine dendritic cells and macrophages, with possible involvement of MCTs.

Lactate, secreted by cervical cancer cells, also modulated the TAM phenotype in a spheroid model with human monocytes [21], enhanced the immunosuppressive phenotype of myeloid-derived suppressor cells (MDSCs) after radiotherapy [22] and increased the frequency of MDSCs generated from mouse bone marrow cells with GM-CSF and IL-6 *in vitro* [23]. A recent study by He et al. showed that activation of the lactate receptor HCAR1 signaling pathway in colorectal cancer cells recruits immunosuppressive CCR2+ PMN-MDSCs [24].

Furthermore, inhibition of tumor glycolysis has been shown to reduce MDSC accumulation, enhance T cell immunity, and suppress tumor growth and metastasis in murine triple-negative breast cancer models, highlighting the crucial role of glycolytic metabolism driving tumor immunosuppression through MDSCs [25].

Interestingly, peripheral polymorphonuclear (PMN)-MDSC correlated with tumor grade in RCC patients and anti-IL1β decreased MDSC in a murine model, suggesting that MDSC inhibition represents a potential target in RCC [26]. Gabrilovich and colleagues identified the lectin-type oxidized LDL receptor-1 (LOX-1) as a specific marker for blood and tumor PMN-MDSC in cancer patients and *OLR1* (LOX-1) expression positively correlated with clinical stage in RCC patients [27].

Additionally, an association between elevated $CD68^+$ TAMs and poor overall survival and progression-free survival [28] suggests that pro-tumorigenic myeloid cells but not T cells are major determinants of patient outcome in ccRCC. In line, Chen et al. demonstrated that TAMs promoted RCC migration, invasion and EMT via IL-6-mediated activation of STAT3 signaling in RCC tumor cells [29]. High concentrations of IL-6 in the TME and blood of RCC patients were correlated with worse survival [30–33] and it has also been shown that macrophages isolated from RCC tumors produce considerable amounts of IL-6 [28]. Interestingly, STAT3 can up-regulate the myeloid-related protein S100A9 and thereby support MDSC differentiation and ROS production [34]. Also, IL-6 blockade has been shown to enhance Th1 differentiation and immune checkpoint blockade in preclinical models of hepatocellular carcinoma and pancreatic cancer [35–39]. Therefore, targeting IL-6 in RCC patients might be a promising strategy.

In this study, we assessed the prognostic value and relationship between lactate metabolism and IL-6 secretion by tumor-associated myeloid cells. We show that myeloid cells, IL-6 and MCT4 levels, but not tumor-infiltrating T cells (TILs) are prognostic for the survival of ccRCC patients and that expression of MCT4 is linked to an immunosuppressive phenotype *ex vivo* and can induce $CD14^+$ HLA-DR low myeloid cells *in vitro*. Targeting glycolysis via the MCT1/4 inhibitor diclofenac or the selective MCT1 inhibitor AZD3965 in combination with the selective MCT4 inhibitor MSC-4381 inhibited lactate and IL-6 secretion in an *in vitro* RCC 3D tumor spheroid co-culture model with infiltrating immune cells and *ex vivo* in patient-derived ccRCC tumoroids. Moreover, metabolic inhibition skews myeloid cells into an immunocompetent phenotype with increased MHC-II and reduced PD-L1 expression.

2. Material and methods

2.1. Chemicals

MCT inhibitors AZD3965 (MCT1 inhibitor) and MSC-4381 (MCT4 inhibitor, Merck Healthcare KGaA, Darmstadt, Germany) were first dissolved in dimethyl sulfoxide (DMSO) at a concentration of 10 mM and further diluted in RPMI1640 to a stock concentration of 100 μM (final concentration used was 0.1 μM of each MCT inhibitor). Diclofenac (Millipore Sigma, Burlington, MA, USA) was dissolved in RPMI1640 at a concentration of 8 mM (final concentration used was 0.2 mM). Roxadustat (Selleckchem, Houston, TX, USA) was dissolved in DMSO to prepare a 100 mM stock solution. For experiments, it was diluted to a final concentration of 25 μM.

2.2. Human ccRCC samples for ex vivo analysis

Fresh malignant tissue was surgically removed from patients with ccRCC. All subjects provided written consent according to protocols approved by the ethical committee of the University Hospital Regensburg (Nr. 16-355-101 and 08/108) in accordance with the Declaration

of Helsinki. In some cases, adjacent healthy kidney tissue was obtained. Patients with confirmed histology of renal oncocytoma, or papillary or chromophobe RCC were excluded from the study. All human samples were first evaluated by a trained pathologist at our institution. The tumor periphery was defined as the region extending from approximately 0 mm (directly at the capsule) to 10 mm from the capsule. Tumor center samples were obtained from areas approximately 20 mm from the capsule and deeper, depending on the overall tumor size. Tissues were processed by mechanical dissociation, followed by enzymatic digestion with DNase and collagenase (Sigma-Aldrich, St. Louis, MO, USA). Single-cell suspension was obtained after passage through a 70-μm strainer and subsequent red blood cell lysis. Fresh single-cell suspensions were cultured for 24h. PMBCs were collected and processed by density gradient centrifugation.

Patients from cohort 1 (n = 10), used in *ex vivo* cultures of single cell suspensions and tumoroids, were: all confirmed clear cell renal carcinoma (ccRCC); mean age 71 years; 40 % female, tumor size T1 in 13 %, T2 in 13 % and T3 in 75 %; tumor grade G1 in 25 %, G2 in 38 %, G3 in 0 % and G4 in 38 %; for two patients, tumor size and grade was not available. Patients from cohort 2 (n = 19), used for mass spectrometry based analysis of lactate, were: all confirmed ccRCC; mean age 63 years; 42 % female; tumor size T1 in 37 %, T2 in 21 %, T3 in 37 % and T4 in 5 %; tumor grade G1 in 0 %, G2 in 74 %, G3 in 26 % and G4 in 0 %.

2.3. Mice and in vivo experiments

Animal experiments were performed according to the regulations of the local government of Würzburg, Germany, and permission was obtained from the Government of Unterfranken, Germany. C57BL/6N mice were purchased from Janvier. All mice used for experiments were 10–12 week old females. To generate B16 tumors in mice, B16.SIY wt or B16.SIY *Ldha/b*$^{-/-}$ cells were harvested, washed and suspended in RPMI Medium (with 10 % FCS), before a 50 μL aliquot containing 0.3 × 10^5 cells was injected subcutaneously into the dorsal region of mice. Every 2–3 days mice were monitored for tumor size and their general condition. Tumor size was estimated by measurements of the short (a) and long (b) axis of the mass and the following formula: l x w^2 x 0,52. At indicated time points mice were sacrificed and tumors were collected. The tissue was digested with a mixture of collagenase type IA and DNase I (Sigma-Aldrich) via injection of the enzymatic cocktail into the tumor mass. During the 45 min incubation, tumors were minced with a scalpel. Afterwards, cells were filtered through a 70 μm cell strainer and ACK lysis was performed to remove erythrocytes from the single cell suspension. Subsequently, flow cytometry analysis was performed as described above.

2.4. Analysis of scRNA seq of murine tumor-infiltrating immune cells

After tumor digestion, immune cells were enriched for CD45 by FACS sorting, loaded onto a 10x Genomics Chromium Next GEM Single Cell 3' Reagent Kits v3.1 and 3′ Feature Barcode Kit (Dual Index) according to the manufacturer's protocol, and sequenced on an Illumina Nextseq 2000 device. Fastq files were processed using Cell Ranger (version 7.0.0) based on 10x Genomics–provided mouse genome mm10 (2020). Downstream analysis was performed using the R package Seurat (version 5.0.1) [40]. Poor quality cells were excluded from downstream analysis with cutoffs for total detected genes >200, >1000 reads and a mitochondrial gene fraction of <5 %. After quality control filtering, 13940 cells were included in the analysis. First, data was normalized ("NormalizeData", normalization.method = "logNormalize"; scale.factor = 1000) and scaled ("ScaleData")and variable features were identified ("FindVariableFeatures", selection.method = "vst"; nfeatures = 2000). After PCA was performed, clustering of cells was conducted ("FindNeighbours", "FindClusters", res = 0.1). Dimension reduction was executed by UMAP projection on the first 20 principal components (dims = 20). Immune cell populations were annotated using the SingleR pipeline [39] with the "MouseRNASeq" (celldex package) dataset as a reference. Celltypes represented with <10 cells were excluded. Subsequently, differential gene expression analysis between the B16 WT and the B16 LDH$^{-/-}$ group was performed on the myeloid cell subset with the "FindMarkers" function (logfc: 0.25, test: wilcox). Genes were ranked according to the average logfold change and gene set enrichment analysis was applied employing the clusterprofiler package [41].

2.5. Bulk and single cell RNA-seq analyses of human data

2.5.1. Analysis of patient single-cell transcriptome data

The dataset that comprised samples from 12 patients with RCC, was sourced from previously published studies by Li R. et al. [42] Dataset [43] and downloaded as AnnData (h5ad) object. Data were imported into Scanpy v1.9.1 and underwent quality control by setting thresholds for the number of detected genes (minimum of 200), counts (minimum of 2000), and the fraction of mitochondrial reads (less than 30 %). Cell transcriptomes were embedded into a batch-corrected low-dimensional latent space using scVI [44,45], with each sample treated as a separate batch. The scVI model was trained on the 2000 most 'highly variable genes' as determined by scanpy's "*pp.highly_variable_genes*' with parameters '*flavor*="*seurat_v3'*, and *batch_key*='*orig.ident'*. A neighborhood graph and UMAP embedding were generated based on the scVI latent representation. All cell-type annotations were adopted from the original publication [42]. For visualization, the integrated UMAP coordinates and annotations were used to generate expression maps and dotplots of selected marker and metabolic genes. Pathway activity was inferred using decoupler-py v.2.1.1 [49] by computing Hallmark gene-set enrichment scores (MSigDB) for glycolysis, IL6_JAK_STAT3_Signaling and Hypoxia. Pseudobulk mean expression profiles were generated on RCC tumor cell population aggregated per patient (with minimum 10 cells per pseudobulk) and correlated with pathway activity score using Kendall's τ (the queried gene was excluded from the pathway score before correlation analysis).

2.5.2. Analysis of young et al. RCC scRNA-seq dataset

Data was downloaded from https://science.sciencemag.org/highwire/filestream/713964/field_highwire_adjunct_files/6/aat1699_DataS1.gz.zip. [46]. Cells were filtered by the authors' QC criteria and subsetted to the 'Tumour Immune Compartment' resulting in 17821 cells. Using the Seurat package (v. 3.2.1) from R, data was normalized (NormalizeData(normalization.method = "LogNormalize", scale.factor = 10000)) and scaled (ScaleData). Subsequently, variable features were identified with the function "FindVariableFeatures(selection.method = "vst", nfeatures = 2000)" and used as input for PCA (RunPCA). Finally, a UMAP representation was calculated based on the first 10 principal components (RunUMAP(dims = 1:10)). Simplified cell annotation labels were created according to the original study by Young et al. [46].

2.6. Analysis of TCGA datasets

Overall survival of papillary renal cell carcinoma (pRCC) patients and clear cell renal cell carcinoma (ccRCC) patients with high and low expression levels of selected genes was analyzed using the R2 dataset: Tumor Kidney Renal Clear Cell Carcinoma - TCGA - 533 - rsem - tcgars (ccRCC) and Tumor Kidney Renal Papillary Cell Carcinoma - TCGA - 290 - rsem - tcgars (pRCC) (http://r2.amc.nl). *SLC16A3*/MCT4 expression in 533 ccRCC patients was plotted against the corresponding *CD14* expression, using the R2: Tumor Kidney Renal Clear Cell Carcinoma - TCGA - 533 - rsem - tcgars dataset. For determination of high and low expression of selected genes, the cut-off modus "scan" divided the patients into two groups. The raw p-value significance was calculated for every graph with the web database. Correlation of selected genes was determined, using the R2 dataset: Tumor Kidney Renal Clear Cell Carcinoma - TCGA - 533 - rsem - tcgars (ccRCC). Pearson's correlation was calculated with the transform 2log setting.

2.7. Tumor cell culture

The human tumor cell lines RJ494 (provided by Prof. Dr. Andreas Mackensen) and HCT116 (ATCC, Manassas, VA, USA), and murine 4T1, B16.SIY wt and $LDH^{-/-}$ cells were cultured in RPMI1640 (Thermo Fisher Scientific, Waltham, MA, USA) supplemented with 10 % FCS (heat-inactivated, Millipore Sigma) and 2 mM L-glutamine (PAN-Biotech, Aidenbach, Germany) in a humidified atmosphere (5 % CO_2, 95 % air) at 37 °C in a Heraeus incubator. The B16.SIY $LDH^{-/-}$ was generated as previously described [47].

2.8. Co-culture of tumor spheroids and immune cells

RJ494/HCT116 spheroids were grown for 4 days with the hanging-drop technique at a density of 1×10^4 cells/30 µL. Spheroids were transferred in 100 µL of fresh medium to ultra-low-attachment plates coated with poly-hema (MilliporeSigma) and incubated for 7 (RJ494)/10 (HCT116) days in the presence or absence of 0.2 mM diclofenac or 0.1 µM MCT1 and MCT4 inhibitor. On day 7/10, lactate levels were determined in culture media (50 µL were removed) and co-culture was started. To approximate the physiological situation, only lysis of erythrocytes from peripheral blood was performed with ACK lysis buffer 1x (6x: 0.155 M NH_4Cl, 0.01 M $KHCO_3$, and 0.1 mM EDTA), and 0.1×10^6/50 µL blood leukocytes were added to spheroid cultures. After 24 h of co-culture, spheroids were picked, non-infiltrated residual immune cells were carefully rinsed away, and single-cell suspensions were generated from pooled spheroids by incubation with trypsin/EDTA (Thermo Fisher Scientific) prior to flow cytometric analysis.

2.9. Differentiation of human myeloid cells

For the *in vitro* generation of human MDSC-like cells, first MNCs were isolated from thrombocyte donation products from healthy individuals via density centrifugation. Alternatively, monocytes were isolated from leukapheresis products via density centrifugation and elutriation. All participants provided written informed consent and the study was approved by the local ethics committee (vote numbers 13-101-0240 and 13-101-0238). MNCs were cultivated at a density of 1.0×10^6 cells/mL in RPMI1640, supplemented with 2 % AB serum, 0.5 % penicillin/streptomycin and 2 mM L-glutamine. For phenotypic analyses of MDSC-like cells, MNCs were incubated for a period of 48 h with respective combinations of recombinant 10 U/mL IL-6 (Peprotech, Rocky Hill, NJ, USA) and 20 mM lactic acid (Sigma-Aldrich) or 20 mM sodium lactate (Sigma-Aldrich) or 25 µM Roxadustat (Selleckchem). To facilitate myeloid cell collection without trypsinization, 12-well plates coated with poly(N-isopropylacrylamide) (PIPAAm; Nunc Upcell, Thermo Fisher Scientific) were used, which enable sample collection after 30–60 min of incubation at 4 °C.

2.10. Suppression assay

$CD3^+$ T cells were isolated from peripheral blood mononuclear cells (PBMCs) of healthy donors using magnetic-activated cell sorting (MACS; Pan T Cell Isolation Kit, human, Miltenyi Biotec). Purified T cells were labeled with 1 µM CellTrace™ Far Red dye (CTFR, Thermo Fisher Scientific) for 20 min at 37 °C and stopped with 5x volume of medium with human serum for 5 min at 37 °C. Labeled T cells were co-cultured with *in vitro*-generated MDSC in 200 µL RPMI1640, supplemented with 2 % AB serum 0.5 % penicillin/streptomycin and 2 mM L-glutamine. Co-cultures were maintained for 4 days in 96-well round-bottom plates (Sarstedt, Nümbrecht, Germany) pre-coated for 2 h at 37 °C with anti-CD3 (1 µg/mL, clone OKT-3, BioLegend, San Diego, CA, USA). T cell proliferation was assessed after 4 days by flow cytometric analysis of CellTrace™ Far Red dye (CTFR) dilution. The percent inhibition was calculated based on the Division Index by comparing the Division Index of treated cells to that of the untreated control.

2.11. Differentiation of murine myeloid cells

For *in vitro* generation of murine MDSC-like cells, first bone marrow was isolated from 10 to 12 week old C57Bl/6 mice. Bone marrow cells were cultivated at a density of 1×10^6 cells/mL in RPMI1640, supplemented with 0.5 % penicillin/streptomycin, 2 mM L-glutamine and 10 % FCS. For phenotypic analyses of bone marrow derived MDSC-like cells, cells were incubated for 7 days with recombinant 10 U/mL IL-6 (Peprotech) and 20 mM lactic acid (Sigma). To facilitate myeloid cell collection without trypsinization, PIPAAm-coated 12-well plates (Nunc Upcell, Thermo Fisher Scientific) were used.

2.12. Determination of cytokines

Cytokine secretion was determined in 24 h culture supernatants by commercially available enzyme-linked immunosorbent assays (R&D Systems, Minneapolis, Minnesota, USA) or the LEGENDplex™ Human CD8/NK V02 Panel (BioLegend) according to the manufacturer's protocol. Data was processed with the LEGENDplex™ Data Analysis Software Suite.

2.13. Quantification of lactate secretion

Tumor cells (2.5×10^4/200 µL) or T cells (0.1×10^6/200 µL) were seeded into flat-bottom 96-well plates for 24 h or 48 h. Lactate concentrations in cell culture supernatants were determined enzymatically by the Department of Clinical Chemistry at the University Hospital of Regensburg, Germany.

For mass-spectrometry based studies, tissue specimens were processed and analyzed as described before [48]. Briefly, samples were weighed and homogenized in cold 80 % methanol and stable isotope-labeled internal standard was added. Upon centrifugation, the supernatant was collected and the remaining pellet was reextracted twice. The combined extract was evaporated to complete dryness for GC-MS analysis of lactate. Quantification was performed using calibration curves, with the corresponding stable isotope-labeled analog serving as internal standard.

2.14. $^{13}C_3$-lactic acid tracing

Human monocytes (4×10^6 cells per well) were seeded in 6-well plates in 4 mL RPMI 1640 medium supplemented with 2 % AB serum, 2 mM L-glutamine, and 0.5 % penicillin/streptomycin. Cells were incubated with $^{13}C_3$-lactic acid for 1h and 24h at 37 °C and 5 % CO_2. After incubation, supernatants were collected and adherent cells were washed three times with ice-cold PBS. Cells were scraped in 600 µL of ice-cold 80 % methanol, transferred to microcentrifuge tubes, and re-scraped with an additional 400 µL of 80 % methanol. Methanolic extracts were combined per sample and stored at −80 °C until analysis. Lactate and pyruvate isotopologue distributions were determined by GC-MS using the method described above. Peak areas for each isotopologue were determined and corrected for natural stable isotope abundance and tracer impurity employing IsoCorrectoR [49]. Data are shown as mean ^{13}C enrichment.

2.15. Monitoring of oxygen consumption in vitro

Cellular oxygen consumption and pH changes in culture medium were determined non-invasively by the PreSens technology (PreSens Precision Sensing GmbH, Regensburg, Germany). 4×10^6 monocytes were seeded in 24-well Oxodish OD24 in 0.5 mL RPMI 1640 medium supplemented with 2 % AB serum, 2 mM L-glutamine, and 0.5 % penicillin/streptomycin under cell culture conditions for the indicated period of time.

2.16. Immunoblotting analysis

Cells were lysed on ice for 30 min in RIPA buffer, followed by centrifugation at 12000 rpm for 20 min at 4 °C. Supernatants were collected and total protein concentrations were determined using the Bicinchoninic acid (BCA) assay kit (ThermoScientific, #23225). Equal amounts of protein were resolved by SDS-PAGE and transferred onto 0.45 μm nitrocellulose membranes (Bio-Rad, #1620115). Membranes were blocked and incubated for 2h at room temperature with anti-L-Lactyllysine (PTM-1401RM; 1:1000 in 5 % non-fat dry milk/TBST). After three 3 min washes in TBST, membranes were incubated for 1 h at room temperature with HRP-conjugated anti-rabbit IgG (Cell Signaling, #7074; 1:1000 in 5 % non-fat dry milk/TBST). Immunoreactive bands were detected using the ChemiDoc Imaging System (Bio-Rad). Membranes were then stripped for 30 min at room temperature using Restore Plus Western Blot Stripping Buffer (Thermo Scientific, #46430), and incubated overnight at 4 °C with anti-β-actin (Cell Signaling, #3700; 1:1000 in 5 % non-fat dry milk/TBST). The following day, membranes were washed and incubated 1h at room temperature with HRP-conjugated anti-mouse IgG (Cell Signaling, #7076; 1:1000 in 5 % non-fat dry milk/TBST). Bands were visualized using the ChemiDoc Imaging System (Bio-Rad).

2.17. Flow cytometry

Single-cell suspensions from spheroid co-cultures were prepared as described above. For live-dead discrimination, cells were stained with 80 μL Zombie-NIR (diluted 1:650 in PBS; BioLegend) or 50 μL Zombie Aqua (diluted 1:200 in PBS; BioLegend) for 10 min at RT in the dark. The Fc Block (BD Biosciences, Franklin Lakes, NJ, USA) was added for 10 min at 4 °C in the dark before surface staining. Human cells were stained with anti-CD45 (BD Biosciences), anti-CD3 (BioLegend), anti-CD14 (BioLegend), anti-CD66b (BioLegend), anti-HLA-DR (BioLegend), anti-PD-L1 (BioLegend), anti-CD33 (BioLegend), anti-CD11b (BD Bioscience)), anti-CD15 (BioLegend), anti-LOX-1 (BioLegend), anti-S100A9 (BioLegend). Intracellular staining of IL-6 (BD Biosciences) and CD68 (BioLegend) was performed for 20 min after fixation/permeabilization using the Fixation/Permeabilization Kit (BD Bioscience) according to the manufacturer's protocol. Intracellular staining of HIF1α (#359706, BioLegend) or isotype control (#400330, BioLegend) was performed after fixation/permeabilization using the eBioscience™ Foxp3/Transcription Factor Staining Buffer Set (Thermo Fisher Scientific). Murine Cells were stained with anti-CD45, anti-CD11b (BioLegend), anti-I-Ab, anti-Gr-1 (BioLegend), anti-Ly6C (BD BioScience), anti-Ly6G (BioLegend). Intracellular staining of pSTAT3 (BioLegend) was performed for 20 min after fixation/permeabilization using the fixation buffer and True-Phos™ Perm Buffer (BioLegend) according to the manufacturer's protocol. Flow cytometry was performed using a BD FACS Celesta or BD FACS Fortessa. Data were analyzed with the FlowJo software (v10.8.1, Tree Star).

2.18. Immunohistochemistry

Routine histology staining (hematoxylin and eosin stain (HE)) was performed following standard protocols. Immunohistology was performed using an automated immunostainer (Ventana Benchmark Ultra, Roche Diagnostics, Mannheim, Germany) with antibodies against CD68 (Dako Cytomation, Glostrup, Denmark, Clone PGM1, Code No. M 0876, 1:200), CD3 (Dako Cytomation, Code No. A 0452, 1: 2000), and GLUT1 (Diagnostic BioSystems, Pleasanton, CA, USA, RP 128, 1:200).

For detection of MCT4+ and CD68 in representative RCC samples, the protocol was conducted with the HiDef Detection™ HRP Polymer-System (Cell Marque™ Rocklin, CA, USA), according to the manufacturers' instructions. Antigen retrieval was performed in 10 mM Tris buffer, 1 mM EDTA, pH 9.0 (CD68) or 10 mM citrate buffer, pH 6.0 (MCT4) in a water bath at 98 °C. Endogenous peroxidase activity was blocked with 3 % hydrogen peroxide in methanol. Anti-CD68 and anti-MCT4 primary antibodies were obtained from Dako (Glostrup, Denmark) and Santa Cruz Biotechnology, Inc. (Dallas, TX, USA); these were both diluted at 1:100 and incubated on the sections for 2 h at room temperature. A liquid 3,3′-diaminobenzidine (DAB) substrate kit (Cell Marque™ Rocklin, CA, USA) was used for staining, before the sections were counterstained with hematoxylin. Negative controls were included by the omission of the primary antibodies. $CD68^+$ tonsil and $MCT4^+$ testicular cancer sections were used as positive controls for CD68 and MCT4 detection, respectively. Immunoreactivity was semi-quantitatively evaluated in hotspot areas for membrane and/or cytoplasmic staining of cancer and immune cells under an Olympus® BX61 (Tokyo, Japan) microscope, using a grading system based on the percentage of stained cells (0, 0 % positive; 1, <5 % positive; 2, 5–50 % positive; 3, >50 % positive) and the intensity of staining (0, negative; 1, weak; 2, intermediate; 3, strong). The sum of percentage and intensity defined the final score (cutoff = 3: score <3 negative and score >3 positive).

2.19. Statistical analysis

Statistical parameters including the exact value of n, the definition of the center, dispersion, and precision and statistical significance are reported in the figures and the figure legends. Statistical analysis was performed with the GraphPad Prism software (version 9 and version 10). Results were considered statistically significant at $p < 0.05$. Correlations were calculated using the Pearson correlation coefficient. For comparisons between two groups, either an unpaired *t*-test or a Mann-Whitney *U* test was used, depending on data distribution. For comparisons involving more than two groups, a one-way ANOVA followed by Šidák's or Tukey's multiple comparison test was applied.

3. Results

3.1. The monocarboxylate transporter MCT4 and $CD14^+$ myeloid cells determine the outcome in ccRCC, but not pRCC patients

Clear cell renal cell carcinoma (ccRCC) driven by VHL loss stands out as the most common and a lethal subtype of RCC, underscoring the importance of dissecting its unique metabolic adaptations [1,2]. Loss of VHL function drives glycolysis in RCC as it leads to HIF1α stabilization [50] which in turn induces glycolytic genes such as *LDHA*, *GLUT1* and *MCT4*. Analysis of TCGA data revealed that ccRCC (KIRC) displayed the highest expression of the lactate transporter MCT4 among all tumor types underscoring the high glycolysis phenotype (Fig. 1A). In addition, there was a positive association between MCT4 (*SLC16A3*) and *CD14* (a marker for tumor-associated myeloid cells) expression in ccRCC patients, and both genes were negatively correlated with survival in ccRCC, but not in papillary renal cell carcinoma (pRCC) patients (Fig. 1B). The same was true for *CD68*, which served as marker for tumor-associated macrophages (Fig. S1A). *CD14* expression in RCC also correlated with other typical myeloid markers such as *S100A8/9* and surprisingly also with LOX-1 (*OLR1*) (Fig. S1B). The latter is a known marker for tumor-associated PMN MDSC [27]. Interestingly, expression of the T cell marker *CD8* had no positive prognostic relevance (Fig. S1A). To clarify whether myeloid cells indeed expressed MCT4 in RCC tissue, we used scRNAseq analysis of RCC tissue and blood samples [42]. Tumor-associated and blood myeloid cells were found to be the cell type with the highest expression of MCT4 (*SLC16A3*) next to RCC tumor cells in two separate cohorts (Fig. 1C/D and S1C, [46]), whereas MCT1 (*SLC16A1*) expression was not restricted to a specific cell type in RCC samples (Fig. 1D).

Based on the high expression of MCT4, we speculated that tumor-associated $CD14^+$ myeloid cells might exhibit high glycolytic activity as it had been shown that myeloid cells contribute to lactate acidosis in the TME [13]. However, neither the main glucose transporter GLUT1

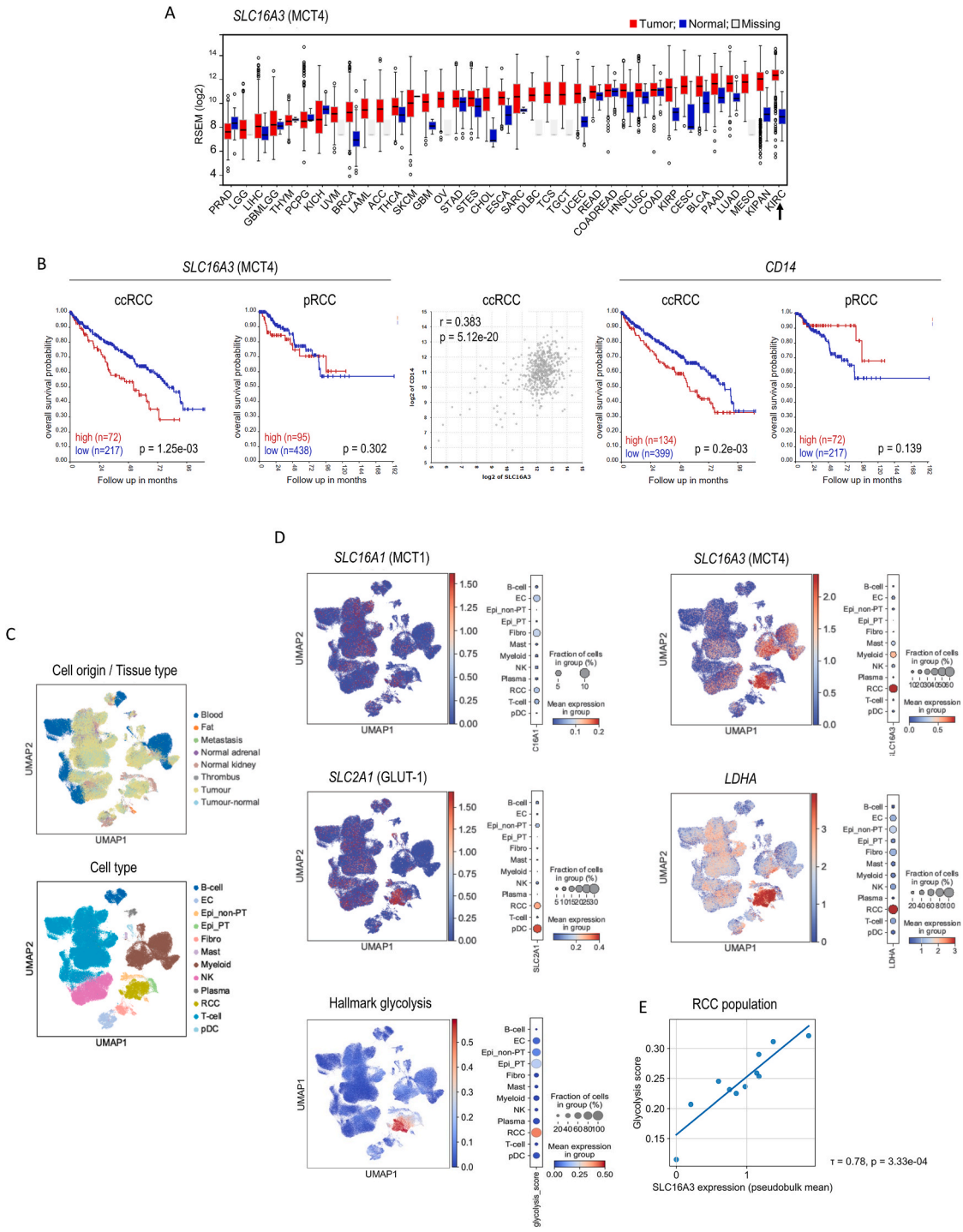

Fig. 1. Monocarboxylate transporter MCT4 and CD14 determine the outcome in ccRCC patients, but not in pRCC patients. **A,** Expression of *SLC16A3* (MCT4), assessed in the cancer genome atlas using FIREBROWSE (http://firebrowse.org/). PRAD: Prostate Adenocarcinoma; LGG: Brain Lower Grade Glioma; LIHC: Liver Hepatocellular Carcinoma; GBM: Glioblastoma Multiforme; THYM: Thymoma; PCPG: Pheochromocytoma and Paraganglioma; KICH: Kidney Chromophobe; UVM: Uveal Melanoma; BRCA: Breast Invasive Carcinoma; LAML: Acute Myeloid Leukemia; ACC: Adrenocortical Carcinoma; THCA: Thyroid Carcinoma; SKCM: Skin Cutaneous Melanoma; OV: Ovarian Serous Cystadenocarcinoma; STAD: Stomach Adenocarcinoma; ESCA: Esophageal Carcinoma; SARC: Sarcoma; DLBC: Lymphoid Neoplasm Diffuse Large B-cell Lymphoma; TGCT: Testicular Germ Cell Tumors; UCEC: Uterine Corpus Endometrial Carcinoma; READ: Rectum Adenocarcinoma; HNSC: Head and Neck Squamous Cell Carcinoma; LUSC: Lung Squamous Cell Carcinoma; COAD: Colon Adenocarcinoma; KIRP: Kidney Renal Papillary Cell Carcinoma; CESC: Cervical Squamous Cell Carcinoma and Endocervical Adenocarcinoma; BLCA: Bladder Urothelial Carcinoma; LUAD: Lung Adenocarcinoma; MESO: Mesothelioma; PAAD: Pancreatic Adenocarcinoma; KIRC: Kidney Renal Clear Cell Carcinoma. **B,** Overall survival of 290 papillary renal cell carcinoma (pRCC) patients and 533 clear cell renal cell carcinoma (ccRCC) patients with high and low expression levels of *SLC16A3* (MCT4) and *CD14*. *SLC16A3* (MCT4) expression in 533 ccRCC patients was plotted against the corresponding *CD14* expression. **C**, UMAP representation of the single-cell dataset showing tissue origin and cell type annotation of major cell populations. **D**, UMAP plots showing expression of *SLC16A3* (MCT4), *SLC16A1* (MCT1), and *LDHA*, *SLC2A1* (GLUT-1), together with the hallmark glycolysis signature and corresponding dotplot summary across annotated cell types. **E,** Correlation between *SLC16A3* expression and glycolysis score in pseudobulked tumor cell populstions (aggregated per patient). Each dot represents one patient. Correlation was assessed using Kendall's τ ($\tau = 0.78$, $p = 3.33 \times 10^{-4}$).

(*SLC2A1*) nor *LDHA* were strongly expressed in the myeloid compartment but were rather restricted to RCC tumor cells (Fig. 1D). MCT4 expression in RCC tumor-cell pseudobulk correlated with a high glycolytic score (Fig. 1E), in line with prior work linking MCT4 to glycolytic metabolism in cancer [9].

3.2. CD14$^+$/HLA-DR low/PD-L1$^+$ cells accumulate in ccRCC tissues and exhibit high IL-6 production

To investigate the amount and activity of CD14$^+$ myeloid cells in ccRCC tumors, we used freshly resected, viable human ccRCC tissues and generated single-cell suspensions for further *ex vivo* analyses (Fig. 2A).

Overall, central and peripheral ccRCC tissue did not show major differences in immune cell infiltration (Fig. 2B). However, RCC tissue showed a higher abundance of CD45$^+$ immune cells compared to adjacent healthy kidney tissue (Fig. 2B). CD3$^+$ T cells accounted for approximately 70 % of CD45$^+$ cells, whereas CD14$^+$ cells averaged about 8 % in viable single-cell suspensions prepared from both tumor and healthy kidney biopsies (Fig. 2B). Myeloid cells in tumors often represent a heterogeneous population. Myeloid-derived suppressor cells (MDSCs), divided into granulocytic CD14$^-$ (G-MDSC) and monocytic CD14$^+$ subtypes (M-MDSC), are an important immunosuppressive subpopulation with low or absent MHC-II expression [51]. Interestingly, in healthy kidney tissue, almost no CD14$^+$ HLA-DR low M-MDSCs were found among CD14$^+$ cells, while their frequencies in central and peripheral tumor tissue increased up to 60 % (Fig. 2B). Furthermore, all CD14$^+$ cells showed expression of the immune checkpoint PD-L1 (Fig. S2A) and about 80 % of the CD14$^+$ cells also expressed CD68 (Fig. S2B). Consistently, the scRNA seq data confirmed that the majority of RCC-associated myeloid cells expressed *CD14* and *CD68* (Fig. S2C). In line with these findings, immunohistochemical analysis of RCC tissues revealed a strong infiltration of CD68$^+$ macrophages, which was associated with high MCT4 expression (Fig. 2C). Moreover, this infiltration correlated with increased GLUT-1 expression in ccRCC tissue compared to adjacent healthy tissue from the same patient (Fig. S2D).

Cytokines, especially IL-6, are known as master regulators of MDSC differentiation [64,65]. Therefore, we analyzed cytokine expression in the supernatants of ccRCC single-cell suspensions by a bead-based multiplex technology. IL-6 expression was highest among all tested cytokines (Fig. 2D). Analysis of IL-6 levels by ELISA in supernatants of cultivated ccRCC and healthy kidney tissues revealed large amounts of IL-6, up to 50.000 pg/mL, in central ccRCC, whereas IL-6 levels in healthy kidney tissue were significantly lower (Fig. 2D). No differences were found for IL-10 (Fig. S2E). IL-6 levels in supernatants from ccRCC tissues positively correlated with the abundance of CD14$^+$ cells and with lactate levels (Fig. 2E). In line, measurement of lactate in 19 additional cryopreserved uncultivated ccRCC tumors showed higher levels in tumor tissues compared to healthy kidney tissue (Fig. 2F). We cultured freshly isolated blood monocytes from healthy donors with lactic acid, which trended toward inducing intracellular IL-6 (Fig. 2G).

Importantly, we identified CD14$^+$ cells as the major producers of IL-6 in ccRCC using single-cell measurements of intracellular IL-6. The complete CD14$^+$ cell fraction (not only the HLA-DR low subpopulation) showed a high expression of IL-6 compared to CD3$^+$ tumor-infiltrating T cells (TILs) and CD45$^-$ tumor cells, and also expressed higher levels of IL-6 than CD14$^+$ cells from healthy kidney tissue (Fig. 2H and data not shown).

Thus, while the CD14$^+$/HLA-DR low cell subpopulation accumulated in ccRCC tumor tissues, all CD14$^+$ cells exhibited high PD-L1 and IL-6 expression. High IL-6 levels were found in tumor supernatants and correlated positively with lactate levels, suggesting a mechanistic relationship of these two factors.

3.3. MCT inhibition reduces lactate and IL-6 levels in RJ494 and HCT116 spheroid co-culture models in vitro

To investigate the metabolic interplay between immune cells and tumor cells at a mechanistic level, we developed a co-culture model, in which immune cells migrated into 3D RCC tumor spheroids derived from the RJ494 tumor cell line (Fig. 3A). Spheroids mimic a TME that forms gradients of hypoxia, nutrients and lactate [52].

To suppress lactate production we incubated RCC tumor cells (monolayer) in the presence or absence of the nonsteroidal anti-inflammatory drug (NSAID) diclofenac, a potent combined MCT and COX inhibitor [41], single selective inhibitors of MCT1 and MCT4 or a combination of MCT1/4 inhibitors (Fig. 3B). Only combined administration of MCT1/4 inhibitors or diclofenac could significantly diminish lactate secretion and was used for further experiments (Fig. 3B).

RCC spheroids were grown for 4 days and then incubated for 7 days in the presence or absence of the NSAID diclofenac, or a combination of MCT1/4 inhibitors (Fig. 3C). On day 7, lactate levels were determined in the culture media and co-culture with immune cells was initiated. To better reflect the physiological environment, whole blood leukocytes, including granulocytes, were added to the spheroid cultures. After 24 h, spheroids were harvested, non-infiltrated immune cells were washed away, and single-cell suspensions were prepared and analyzed by flow cytometry.

The morphology of RJ494 spheroids was not affected by treatment or after co-culture with immune cells (Fig. 3C). Immune cell infiltration in RJ494 spheroids displayed high donor-dependent variation from 13 % to 70 % infiltrated CD45$^+$ cells, but the abundance of immune cells was not significantly altered by treatment with diclofenac or MCT inhibitors (Fig. 3D). Interestingly, similar to RCC patient tumor samples (Fig. 2), CD3$^+$ T cells represented the largest proportion of infiltrating immune cells (approximately 45 %, data not shown). In line with published data and experiments in monolayer cultures [48,53], lactate secretion of RCC tumor spheroids was strongly decreased by diclofenac and selective MCT1/4 inhibitors (Fig. 3D).

Since the analyses of tumor tissues identified IL-6 as an interesting CD14$^+$ cell-derived cytokine (Fig. 2H), we examined IL-6 expression in spheroid co-cultures. Importantly, in line with human ccRCC tissues, RCC spheroid-infiltrating CD14$^+$ cells showed high intracellular levels of IL-6. The lowest IL-6 expression was found in spheroid-infiltrating T cells (Fig. 3E). Notably, IL-6 levels in the culture supernatants of the RCC co-culture model were reduced by diclofenac and MCT1/4 inhibition (Fig. 3F).

Since tumor infiltrating CD14$^+$ cells in patient tumors were characterized by high PD-L1 and an increased low HLA-DR expressing population, we analyzed these markers in the RCC co-culture model. The antigen presenting molecule HLA-DR was significantly upregulated by diclofenac and selective MCT1+4 inhibition (Fig. 3G). Similarly, the immune checkpoint ligand PD-L1 was downregulated upon MCT1+4 inhibition (Fig. 3H).

Thus, MCT inhibition decreased IL-6 production and reverted the PD-L1 high/HLA-DR low phenotype of tumor infiltrating CD14$^+$ myeloid cells.

To analyze the impact of MCT inhibition in a second glycolytic tumor type, we used a co-culture model with immune cells migrating into 3D colorectal carcinoma (CRC) HCT116 tumor spheroids (Fig. S3A). Similar to the observations in RCC, MCT inhibition slightly improved immune cell infiltration (Fig. S3B) and decreased lactate secretion (Fig. S3C). In this model, diclofenac treatment resulted in a smaller spheroid size compared to control even before co-culture of HCT116 tumor spheroids with immune cells (Fig. S3A). Interestingly, in contrast to the RCC spheroid model, CD66b$^+$ neutrophils represented the largest proportion of the immune cell infiltrate with approximately 65 %, compared to approximately 25 % CD3$^+$ TILs. After treatment with MCT inhibitors or diclofenac, there was a trend towards increased numbers of CD14$^+$ cells and a slight reduction in neutrophils, but no clear changes in the T cell

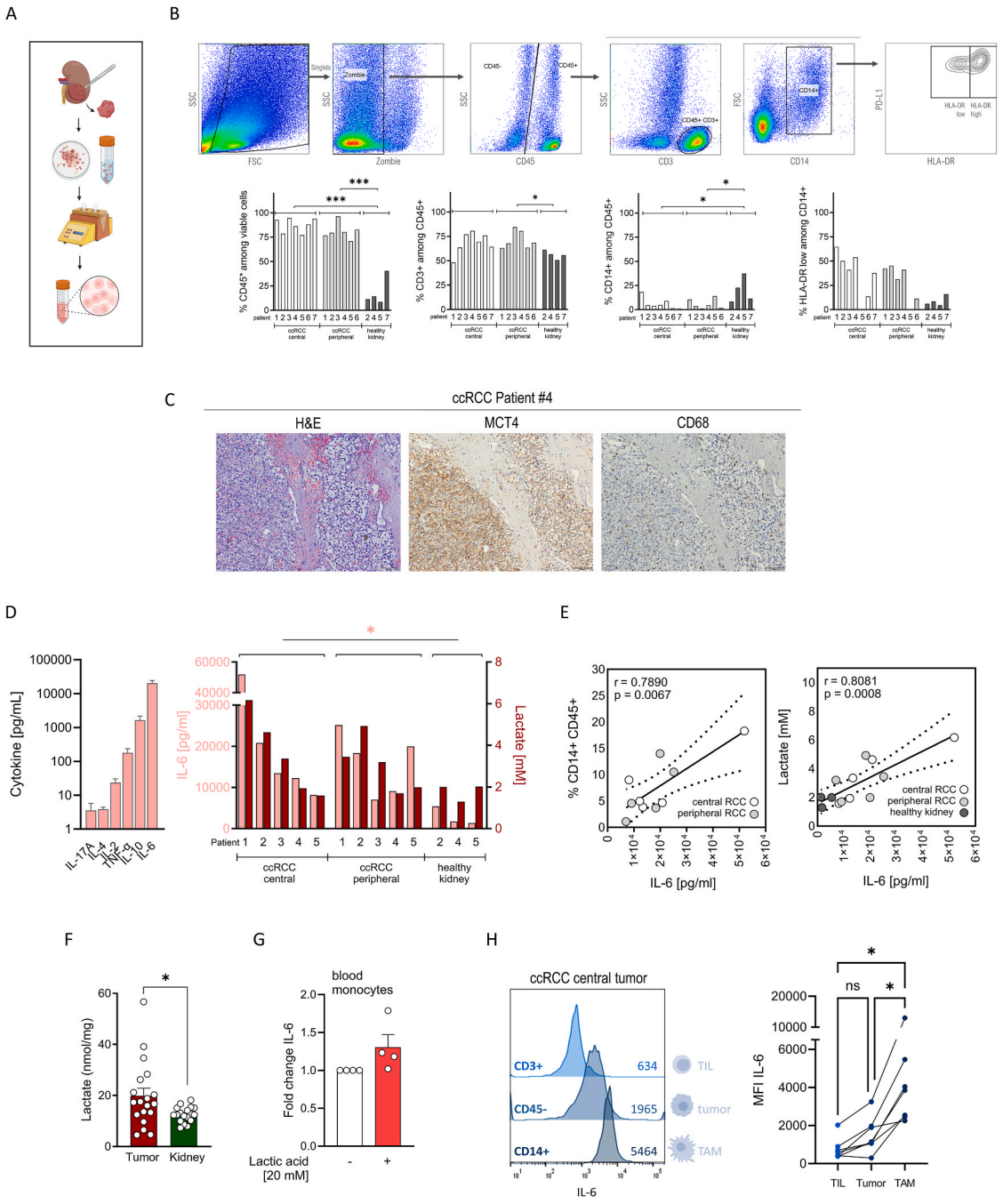

Fig. 2. CD14^{+}/HLA-DR low/PD-L1^{+} cells accumulate in ccRCC tissues and exhibit elevated IL-6 production. **A,** Schematic overview of the preparation of single-cell suspensions from ccRCC tissues (illustration created with BioRender.com). Tumor and kidney biopsies were minced and dissociated both mechanically and enzymatically. After 24 h, the cells were analyzed by flow cytometry. **B,** Gating strategy for flow cytometry analysis: Live cells were identified as Zombie-negative, leukocytes as CD45^{+}, TILs as CD3^{+}, TAMs as CD14^{+}. HLA-DR low TAMs were gated as CD14^{+} and HLA-DR low. Representative flow cytometry plots from a single experiment are shown. The frequencies of TILs (CD3^{+}) and TAMs (CD14^{+}) among CD45^{+} cells, as well as HLA-DR low TAMs among CD14^{+} cells, are displayed. Each column represents an individual patient. Statistical significance was determined using one-way ANOVA followed by Šidák's post-hoc multiple comparison test (*p $<$ 0.05, ***p $<$ 0.001). **C,** Representative H&E and immunohistochemical stains for MCT4 and CD68 of tumor tissue sections from patient #4. Images shown at 100x magnification. **D,** Cytokine and lactate concentrations secreted by ccRCC tumors and healthy kidney tissue. Cytokine profile (IL-17A, IL-4, IL-2, TNF, IL-10 and IL-6 levels) of ccRCC tumors was analyzed in culture supernatants after 24 h using a bead-based multiplex assay. Lactate concentrations and IL-6 determined by ELISA were measured in the same culture supernatants after 24 h. Statistical significance was determined using one-way ANOVA followed by Šidák's post-hoc multiple comparison test (*p $<$ 0.05). **E,** Correlation between donor-matched IL-6 levels and CD14^{+} cell counts or lactate concentrations in single cell suspensions of ccRCC. Correlations were assessed using Pearson's correlation test. **F,** Lactate concentration in cryopreserved ccRCC tumor and corresponding normal kidney tissues, determined using mass spectrometry. Statistical significance was determined using paired *t*-test (*p $<$ 0.05). **G,** Fold change of intracellular IL-6 expression in human monocytes treated with or without lactic acid (Mean +SEM with individual data points are shown). **H,** IL-6 expression in tumor and immune cells derived from ccRCC tumors. IL-6 expression was analyzed by flow cytometry. One representative histogram showing tumor cells (CD45^{-}), TILs (CD3^{+}), and TAMs (CD14^{+}) and data from seven individual patients after 24 h of culture are displayed. Statistical significance was assessed using one-way ANOVA followed by Šidák's post-hoc multiple comparison test (*p $<$ 0.05). MFI, median fluorescence intensity.

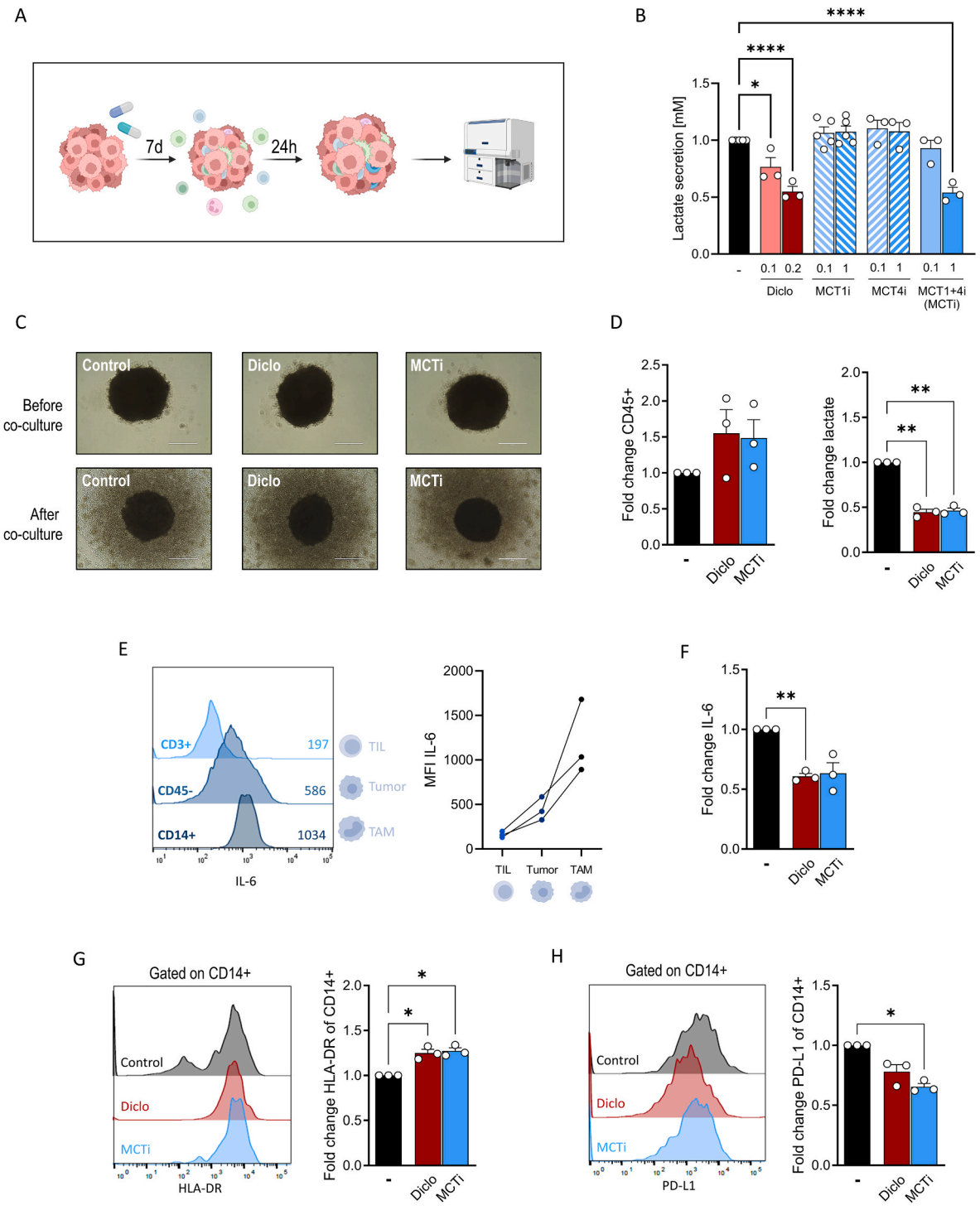

Fig. 3. MCT inhibition reduces lactate and IL-6 levels in RJ494 spheroid co-cultures models *in vitro*. **A,** Schematic overview of the co-culture protocol (illustration created with BioRender.com). RJ494 (RCC cell line) spheroids were treated with MCT inhibitors for 7 days, after which freshly isolated immune cells from the peripheral blood of healthy donors were added to the culture for 24 h. After co-culture, spheroids were harvested, pooled, washed, and prepared for subsequent flow cytometry analysis. Spheroids were treated with either 0.2 mM diclofenac (Diclo) or 0.1 μM MCT1+4 inhibitor (MCTi). Representative images of tumor spheroids before and after co-culture with whole-blood leukocytes are shown. **B,** Fold change in viable $CD45^+$ infiltrated immune cells after 24 h of co-culture. **C,** Fold change in lactate concentrations in culture supernatants, measured after 7 days. **D,** IL-6 expression in RJ494 tumor spheroids after 24 h of co-culture. IL-6 expression was analyzed by flow cytometry. One representative histogram showing tumor cells ($CD45^-$), TILs ($CD3^+$), and TAMs ($CD14^+$) and data from three individual experiments are displayed. MFI, median fluorescence intensity. **E,** IL-6 levels in culture supernatants, measured by ELISA after 24 h of co-culture. **F,** Fold change of HLA-DR expression in viable infiltrated $CD14^+$ TAMs among $CD45^+$ leukocytes, determined by flow cytometry after 24 h of co-culture. **G,** Fold change of PD-L1 in viable infiltrated $CD14^+$ TAMs among $CD45^+$ leukocytes, determined by flow cytometry after 24 h of co-culture. **B, C, D, E, F, G, H** Statistical significance was assessed using one-way ANOVA followed by Tukey's post-hoc multiple comparison test ($^*p < 0.05$). In bar graphs, mean +SEM and individual data points are shown, with statistical significance assessed using one-way ANOVA followed by Tukey's post-hoc multiple comparison test ($^*p < 0.05$,$^{**}p < 0.01$, $^{****}p < 0.0001$).

fraction (data not shown).

In the CRC co-culture model, HCT116 tumor cells showed the highest IL-6 production, followed by CD14$^+$ cells (Fig. S3D). Similar to lactate, IL-6 levels were strongly reduced by diclofenac and by selective MCT1+4 inhibition (Fig. S3E). Furthermore, we confirmed an elevated expression of HLA-DR upon treatment with diclofenac and MCT1/4 inhibitors, but no clear effect on PD-L1 (Fig. S3F and S3G).

Overall, the lactate efflux from RCC and HCT116 spheroids was

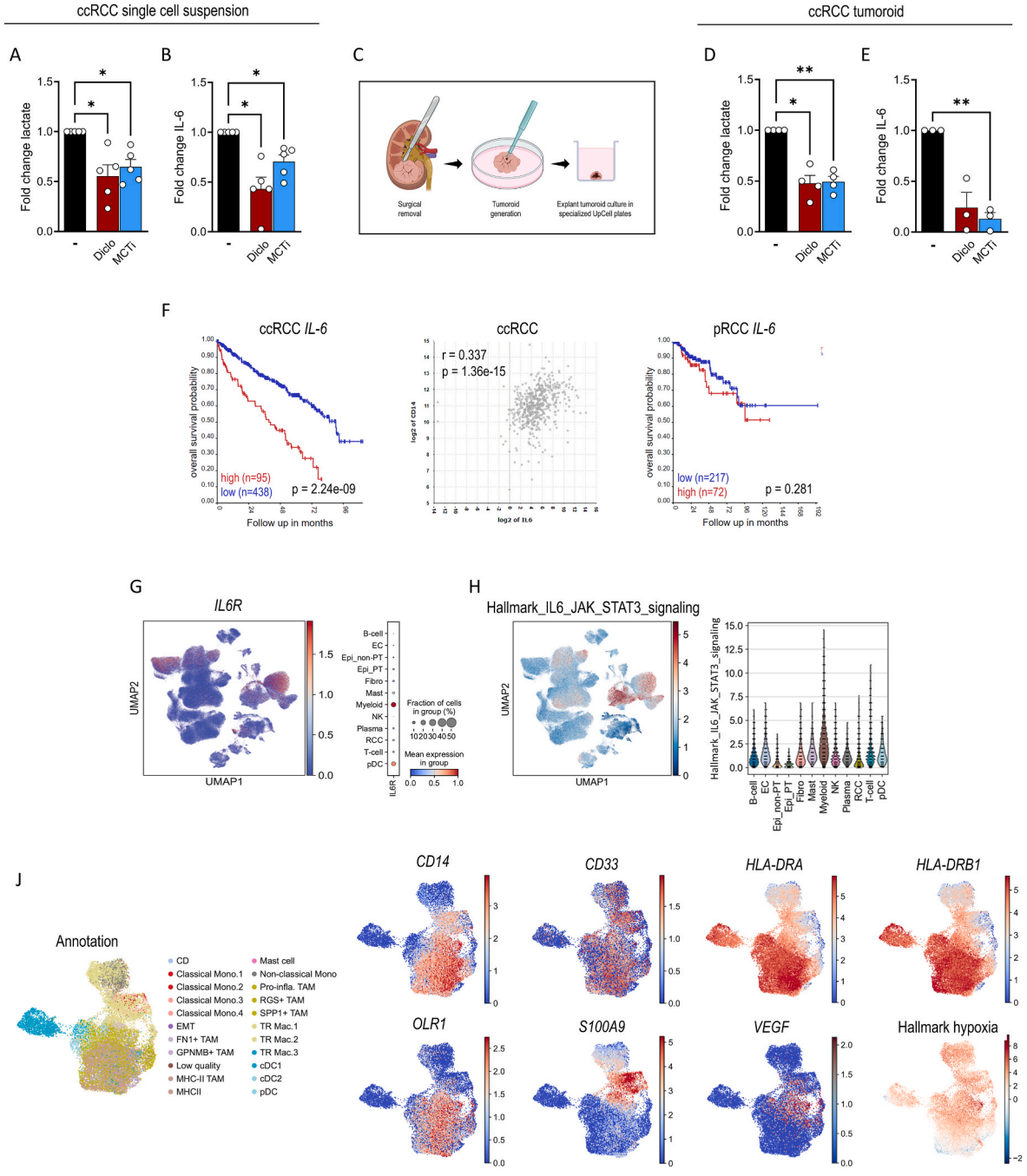

Fig. 4. MCT inhibition limits lactate and IL-6 in primary tumor cell cultures. **A, B,** Tumor biopsies were mechanically and enzymatically dissociated, then cultured with either 0.2 mM diclofenac (Diclo) or 0.1 μM MCT1+4 inhibitors (MCTi) for 24 h. **A,** Fold change in lactate concentrations, measured in the culture supernatants of single-cell suspensions. **B,** IL-6 levels were analyzed in the supernatants by ELISA. **C,** Fresh tumor samples were minimally processed into uniformly-sized tumoroids without chemical dissociation or reassembly. Wet weight was measured before culture for normalization. The schematic illustration was created with BioRender.com. **D,** Lactate concentrations in the culture supernatants were measured after 48 h of treatment with either 0.2 mM diclofenac (Diclo) or 0.1 μM MCT1+4 inhibitors (MCTi), and IL-6 levels in the supernatants were determined by ELISA. **A, B, D, E,** Mean +SEM with individual data points are shown. Statistical significance was assessed using one-way ANOVA followed by Tukey's post-hoc multiple comparison test (*$p < 0.05$, **$p < 0.01$). **F,** Overall survival of 533 clear cell renal cell carcinoma (ccRCC) patients with high and low expression levels of IL-6 expression levels. Correlation of *IL-6* expression and the corresponding *CD14* expression in 533 clear cell renal cell carcinoma (ccRCC) patients. Overall survival of 290 papillary renal cell carcinoma (pRCC) patients. **G,** UMAP visualization showing *IL6R* (IL-6 receptor) expression across cells, with corresponding dot-plot summary. **H,** UMAP plots showing hallmark IL-6/JAK/STAT3 signaling pathway activity and the corresponding violin plot. **J,** UMAPs depicting annotated RCC-associated myeloid populations and expression of *CD14*, *CD33*, *HLA-DRA*, *HLA-DRB1*, *OLR1* (LOX-1), *S100A9*, *VEGF*, and hallmark genes associated with hypoxia.

inhibited through MCT blockade with diclofenac and selective MCT1/4 inhibitors. While MCT1 and MCT4 blockade exerted no statistically significant effect on overall immune cell infiltration, IL-6 secretion was clearly diminished. In CD14^{+} cells, MHC-II was upregulated in both models, and PD-L1 was downregulated in RCC co-cultures by MCT inhibition indicating a polarization toward an immunocompetent phenotype.

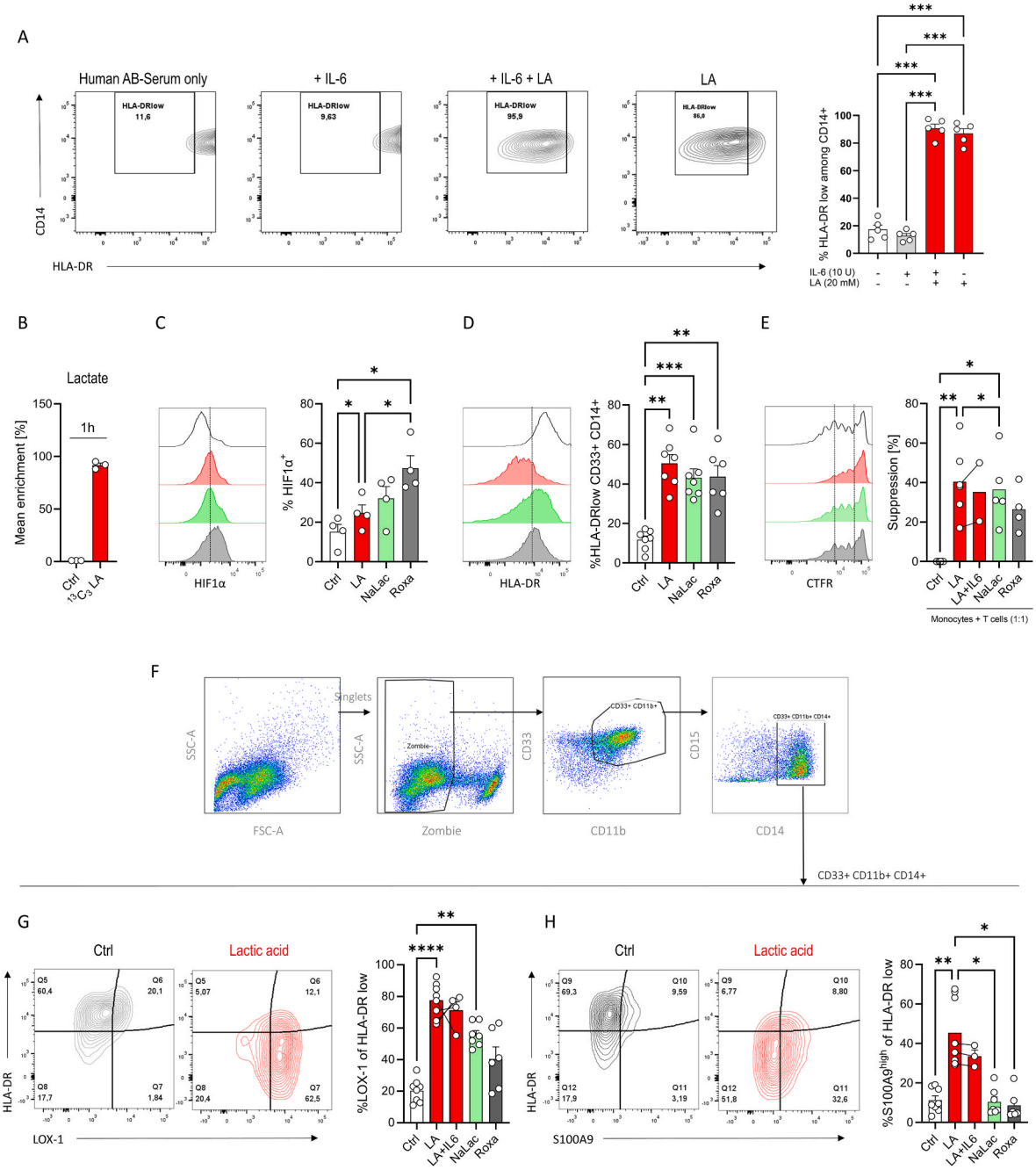

Fig. 5. IL-6 and lactic acid drive the development of an M-MDSC-like phenotype *in vitro*. MNCs from healthy donors were differentiated into MDSC-like cells over 48 h in the presence of human AB serum, IL-6 (10 U), lactic acid (20 mM). Cells were analyzed by flow cytometry using markers (CD14, CD11b, HLA-DR) recommended for human MDSC characterization. **A,** HLA-DR expression in CD14^{+}CD11b^{+} myeloid cells. HLA-DR low MDSC-like cells were gated as CD14^{+} and HLA-DR low cells. Representative flow cytometry plots from a single experiment are shown. The frequencies of HLA-DR low cells are displayed. **B,** Lactate uptake was determined in monocytes cultures after 1 h incubation with $^{13}C_3$-labeled lactic acid. **C**, Intracellular HIF1α was measured in CD14^{+}CD11b^{+} CD33^{+} cells by flow cytometry in human monocytes treated for 12 h with 20 mM lactic acid, 20 mM sodium lactate, or 25 μM Roxadustat. **D,** HLA-DR expression was analyzed in CD14^{+}CD11b^{+} CD33^{+} cells after 48 h. **E,** T cell suppression was assessed by culturing activated T cells at a 1:1 ratio with MDSC-like cells that had been cultured for 72 h with 20 mM lactic acid, lactic acid plus 10 U IL-6, 20 mM sodium lactate, or 25 μM Roxadustat. **F,** Gating strategy for human MDSC-like cells. Cells were first gated on singlets, dead cells were excluded using a Zombie viability dye. Live cells were then gated on CD33^{+}CD11b^{+} myeloid cells. From this population, CD14^{+}CD15^{-}monocytes were selected for characterization of HLA-DR low CD33^{+} CD11b^{+}CD14^{+} MDSC-like cells. **G,** The expression of HLA-DR low LOX-1^{+} cells was determined. H, In parallel, S100A9 expression of HLA-DR low cells was analyzed. **A-H,** Mean +SEM are shown, each symbol represents an individual donor. Statistical significance was determined using one-way ANOVA followed by Tukey's post-hoc multiple comparison test (*p < 0.05, **p < 0.01, ***p < 0.001).

3.4. MCT inhibition limits lactate and IL-6 production in primary tumor cell cultures

Based on our results with spheroid co-culture models, we investigated the impact of MCT inhibition in primary human ccRCC single-cell cultures and ccRCC tumoroids. In line with previous results, MCT inhibition reduced lactate efflux (Fig. 4A) and IL-6 secretion (Fig. 4B) in single-cell suspensions derived from ccRCC tumor tissues. As the characteristics of the TME might be partially lost during tumor dissociation, we aimed to study the impact of MCT inhibition in tumoroids. Tumoroids are patient-derived tumor biopsies with intact TME generated by fresh processing of tumor tissues into equal-sized fragments of about 30 mg without chemical dissociation. Tumoroids were treated for 48 h with MCT inhibitors (Fig. 4C). Again, diclofenac and combined MCT1+4i treatment attenuated lactate secretion of ccRCC tumoroids by about 50 % (Fig. 4D) and suppressed IL-6 secretion (Fig. 4E).

Next, bulk and single-cell transcriptomes of ccRCC tumors were assessed. In line with the *in vitro* analyses, IL-6 expression in RCC patients correlated with *CD14* expression and was a strong negative prognostic indicator in ccRCC but not pRCC patients (Fig. 4F). Interestingly, mainly myeloid cells expressed high levels of the IL-6 receptor (Fig. 4G) and hallmark analyses revealed that the gene signature IL-6/JAK/STAT3 signaling pathway was enriched in tumor-associated myeloid cells (Fig. 4H). Next, we re-clustered the tumor-associated myeloid cells for more detailed characterization, revealing *CD14* expression overlapping with *CD33* in the UMAP analysis. Among *CD14*$^+$/*CD33*$^+$ myeloid cells only a portion of cells strongly expressed *HLA-DRA* and *HLA-DRB1*. Myeloid cells with *S100A9* and *VEGF* expression were mainly found among *HLA-DR* low cells whereas *ORL1* (LOX-1) positive cells and a hypoxia signature were detected in both *HLA-DR* low and high myeloid populations (Fig. 4J).

In summary, in line with previous experiments, MCT-blockade decreased IL-6 production in primary human ccRCC tissues. Furthermore, these data indicate that autocrine or paracrine IL-6 and lactate signaling might determine myeloid cells in the tumor environment which co-express lactate transporters and IL-6 receptors (Figs. 1D and 4G).

3.5. IL-6 and lactic acid promote an MDSC-like phenotype in both humans and mice

To investigate the impact of tumor-derived lactate and IL-6 on myeloid cell differentiation, we cultured human mononuclear cells (MNCs) in the presence of human serum, IL-6, lactic acid or a combination of IL-6 and lactic acid. The cells were analyzed by flow cytometry using markers recommended for the characterization of human MDSC-like cells [51] (gating strategy shown in Fig. S4A). Co-culture with IL-6 and 20 mM lactic acid resulted in approximately 80 % CD14$^+$ HLA-DR low cells compared to only 10–13 % observed with serum alone or serum and IL-6. Surprisingly, lactic acid alone had a similar effect (Fig. 5A). To study the underlying mechanism, we incubated monocytes with $^{13}C_3$-labeled lactic acid. As early as 1 h after start of the culture, labeled lactic acid was detected intracellularly in human monocytes (Fig. 5B). Flux analyses revealed metabolism of lactate to pyruvate which coincided with strongly increased oxygen consumption (Fig. S4B/C). Since it had been shown in murine macrophages that lactate stabilized HIF1α [19], we studied whether lactate uptake would also stabilize HIF1α in human myeloid cells. Roxadustat (Roxa), a HIF-Prolylhydroxylase inhibitor, was used as a positive control and strongly stabilized HIF1α (Fig. 5C). Lactic acid significantly stabilized HIF1α, however to a lesser degree than Roxadustat (Fig. 5C). As HIF1α lactylation has been implicated in its stabilization, we also measured global lactylation and detected a strong effect of lactate and lactic acid (Fig. S4D).

Next, we analyzed whether HIF1α stabilization is involved in the differentiation of the HLA-DR low phenotype in human MDSC-like cells. Similar to lactic acid, Roxadustat induced a MDSC phenotype with low HLA-DR expression (Fig. 5D) and suppressive activity of MDSC was supported by sodium lactate, lactic acid and Roxa (Fig. 5E).

We then studied other markers which have been implicated in the MDSC phenotype (gating strategy in Fig. 5F). LOX-1 expression was increased by lactate and lactic acid and also Roxadustat had a stimulatory effect by trend (Fig. 5G). The calcium binding protein S100A9 was also induced by lactic acid but not Roxadustat (Fig. 5H) and IL-6 had no additive effect on S100A9 expression.

Next, we aimed to translate these findings into a murine model. Murine bone marrow cells were cultured in the presence of FCS, IL-6, and lactic acid and analyzed by flow cytometry using markers recommended for the characterization of murine MDSC-like cells [51]. Notably, 20 mM lactic acid alone or in combination with IL-6 increased significantly the proportion of Gr-1$^+$ cells after 7 days of differentiation compared to the control or IL-6 alone (Fig. 6A). This effect was mainly attributed to upregulation of Ly6G (Fig. S5A).

Based on the *in vitro* results, we extended our findings to an immunocompetent mouse model. The study was conducted with two melanoma B16 cell clones: a wildtype (WT) clone with high lactate secretion and a *Ldha/b* double knockout (*Ldh* DKO) clone with no lactate secretion (Fig. 6B). Tumor growth was significantly delayed in *Ldh* DKO tumor cells (Fig. 6C). Therefore, tumors were harvested at appropriate time points to ensure equivalent tumor size and to exclude an impact of tumor size on immune cell distribution. Tumors were excised, digested and analyzed by scRNAseq analyses. We concentrated on myeloid cells and analyzed *Cd14*, *Cd33*, as well as *I-Ab*, MCT1/4 (*Slc16a1/Slc16a3*), LOX-1 (*Olr1*), *S100a8/9*, *Vegf*, and the hypoxia signature and IL-6/pSTAT3 signaling pathway (Fig. 6D/E). *H2ab* (I-Ab), LOX-1 (*Olr1*), *S100a8/9* and MCT4 were expressed on a portion of *Cd14* myeloid cells (Fig. 6D). Myeloid cells with higher *S100A8/9* expression were characterized by enhanced IL-6/pSTAT3 signaling (Fig. 6E) and gene enrichment analysis showed decreased IL-6/pSTAT3 signaling in *Ldh* DKO tumors (Fig. 6F). In parallel, tumor-infiltrating cells were analyzed by flow cytometry (gating strategy in Fig. S5B). While the total number of myeloid cells was not significantly different between WT and *Ldh* DKO tumors (Fig. S5C), we observed a lower proportion of Gr-1$^+$ MDSCs in the low-lactate *Ldh* DKO tumors compared to the wildtype (Fig. 6G). Gr1$^+$ cells were characterized by a low I-Ab expression (Fig. S5D). In addition, the levels of phosphorylated STAT3 (pSTAT3) in Gr-1$^+$ myeloid cells were significantly reduced in *Ldh* DKO tumors (Fig. 6H), implying decreased IL-6/pSTAT3 signaling. This effect was not found in total CD11b$^+$ myeloid cells (Fig. S5E). Moreover, we assessed cytosolic reactive oxygen species (ROS) levels and observed a trend toward increased ROS in Gr-1$^+$ myeloid cells in B16 WT tumors (Fig. 6I), while total CD11b$^+$ myeloid cells showed significantly elevated ROS levels compared to those from *Ldh* DKO tumors (Fig. S5F), indicating that a high lactate tumor environment may promote ROS accumulation.

Thus, decreased lactate concentrations through genetic manipulation of tumor cells lead to low MDSC frequencies and decreased pSTAT3 signaling in a murine model.

4. Discussion

Since the pioneering work by Galon on the positive correlation between type, density, and location of immune cells within the tumor and patient survival in colorectal carcinoma [54], several studies and meta-analyses have confirmed that TILs are prognostic in many tumor entities [55]. Paradoxically, however, even though RCC is considered as an immunogenic tumor, containing large amounts of TILs, increased mononuclear cell infiltration and tumor-infiltrating PD-1$^+$ immune cells predict an adverse outcome for patients with RCC tumors [56,57]. Tumor-derived factors such as PD-L1 might render T cells dysfunctional, and VHL mutations promote a glycolytic phenotype with lactate accumulation that limits T cell function [13,58,59].

Myeloid cells also contribute to immunosuppression [60]. CD14$^+$

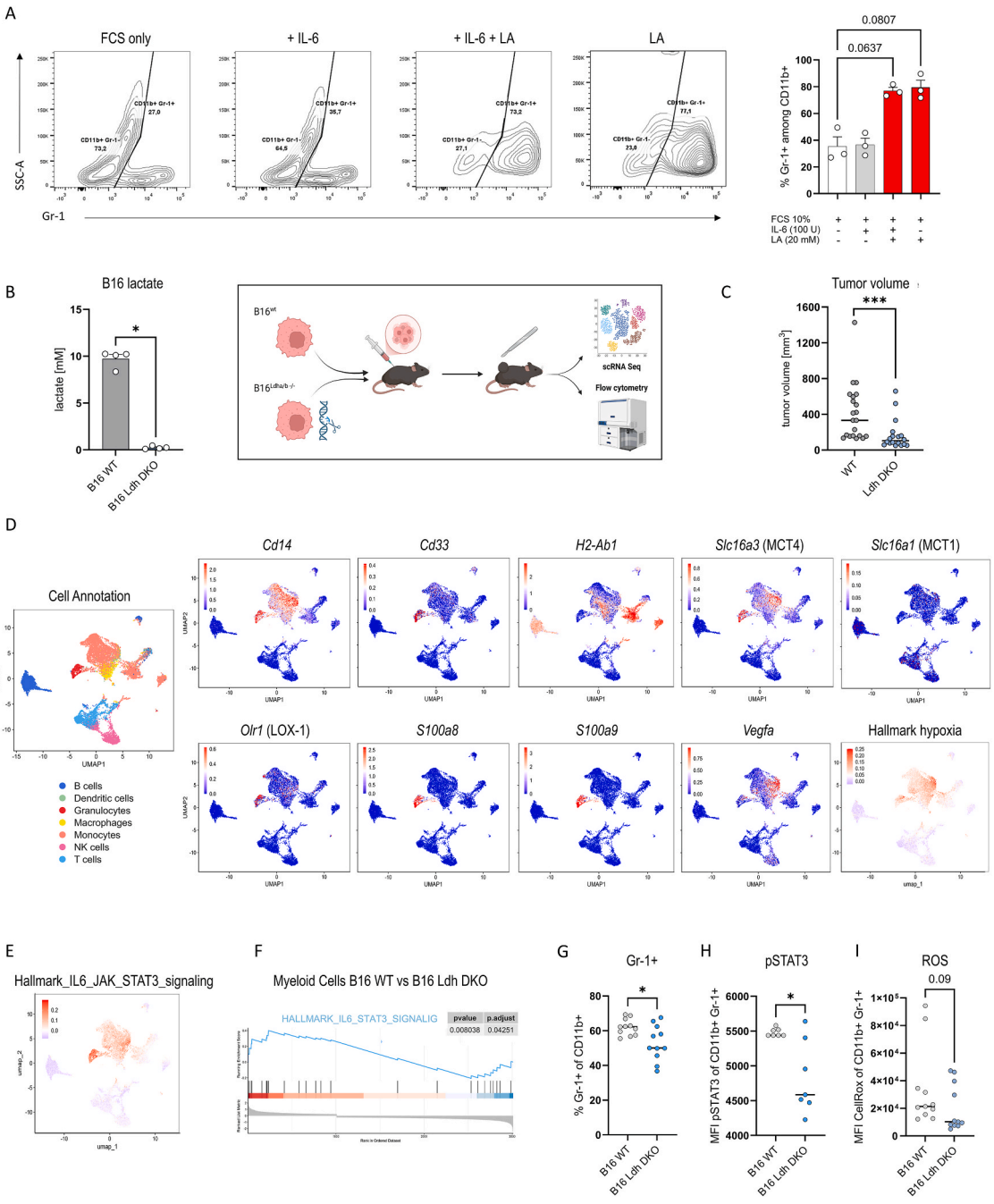

Fig. 6. High lactic acid environment promotes the development of murine Gr-1$^+$ myeloid cells *in vitro* and *in vivo*. **A,** Bone marrow cells isolated from C57BL/6 mice were differentiated into MDSC-like cells over 7 days in the presence of IL-6 (10 U), lactic acid (20 mM) or lactic acid plus IL-6. Cells were analyzed by flow cytometry using markers recommended for murine MDSC characterization (CD11b and Gr-1). Representative flow cytometry plots from a single experiment are shown. The frequencies of CD11b$^+$Gr-1$^+$ cells were quantified. Each symbol represents an individual mouse. Statistical significance was determined using one-way ANOVA followed by Tukey's post-hoc multiple comparison test (*p $<$ 0.05). **B,** Experimental setup for *in vivo* studies. Lactate was measured in B16 WT cells and B16 cells with *Ldha/b* double knockout (DKO) before injection into mice. Mean +SEM and individual data points are shown, with statistical significance assessed using a Mann-Whitney *U* test. (*p $<$ 0.05). To generate B16 tumors in mice, 0.3 $\times$ 10^5 B16.SIY wild-type (wt) or B16.SIY *Ldha/b*$^{-/-}$ tumor cells were injected subcutaneously into the dorsal region of C57BL/6 mice. Tumors were collected on days 12–16 and processed for flow cytometric and scRNA seq analyses. Created with BioRender.com. **C,** Tumor volume on day 11 before the first tumors were dissected. Statistical significance was determined using a Mann-Whitney *U* test. (***p $<$ 0.001). **D,** UMAP depicting clusters of single-cell data with cell type annotation of the major cell types and UMAP plots indicating expression of *Cd14*, *Cd33*, *H2-Ab1, Slc16A3* (MCT4), *Slc16A1* (MCT1), *Olr1* (LOX-1),*S100a8*, *S100a9, Vegfa* and hallmark genes associated with hypoxia. E, UMAP showing hallmark genes associated with the IL-6/JAK/STAT3 signaling pathway. **F,** gene enrichment analyses of hallmark genes associated with the IL-6/JAK/STAT3 signaling pathway in B16 WT vs B16 *Ldha/b* DKO. **G,** Quantification of tumor-infiltrating myeloid cells. The frequencies of CD11b$^+$ and CD11b$^+$Gr-1$^+$ myeloid cells were assessed by flow cytometry. Each symbol represents an individual mouse. Statistical significance was determined using an unpaired *t*-test (*p $<$ 0.05). **H,** Phosphorylation levels of STAT3 (pSTAT3) in CD11b$^+$Gr-1$^+$ myeloid cells were determined by flow cytometry. Median fluorescence intensity (MFI) values are shown, with each symbol representing an individual mouse. **I,** Cytosolic reactive oxygen species (ROS) were measured in CD11b$^+$Gr-1$^+$ myeloid cells using CellROX staining and flow cytometry. Median fluorescence intensity (MFI) values are shown, with each symbol representing an individual mouse. G-I, Statistical significance was assessed using the Mann-Whitney *U* test (*p $<$ 0.05).

HLA-DR low/negative monocytes and CD68$^+$ TAMs correlate with decreased survival and enhanced angiogenesis in RCC [61–63]. Yet the connection between high tumor glycolysis and myeloid-cell-mediated immunosuppression in RCC has remained unclear. A recent study examined the interactions between glycolytic metabolism and myeloid cells in triple-negative breast cancer (TNBC), showing that tumor glycolysis regulates the expression of G-CSF and GM-CSF, which ultimately controls MDSC development and anti-tumor immunity [25].

Moreover, to our knowledge, the antineoplastic activity of anti-metabolic drugs, such as lactate transport inhibitors, on TAMs or MDSCs has not yet been investigated in ccRCC. Here we elucidated how tumor glycolysis shapes myeloid cell function in ccRCC and identified MCT inhibition as a potential therapeutic strategy.

CcRCC tumors were heavily infiltrated by immune cells, predominantly T cells, compared to healthy kidney tissue. Among myeloid cells, CD14$^+$ HLA-DR low/negative cells dominated. These cells have been previously associated with decreased patient survival in RCC patients [62]. Our RJ494 spheroid co-culture reproduced this phenotype, confirming its value as a physiological RCC model.

Based on surface markers alone, it cannot be distinguished whether CD14$^+$ HLA-DR low cells belong to the macrophage lineage or rather resemble the MDSCs. Therefore, we analyzed the functional phenotype of tumor-infiltrating myeloid cells. As myeloid cells are a prominent source of IL-6 and high expression of IL-6 in the TME correlates with worse survival, we measured IL-6 in single-cell patient-derived RCC cultures. We detected high levels of IL-6 in the supernatant of RCC biopsy cultures, and IL-6 concentration correlated positively with the number of myeloid cells. In line, in RJ494 spheroid co-cultures with immune cells, we identified myeloid cells as the major source of IL-6 whereas in the CRC co-culture, tumor cells produced more IL-6.

IL-6 is a key player in the regulation of MDSC activity [64,65], and its targeting enhances T cell responses and ICB efficacy [35–39]. Secretion of IL-6 by tumor cells and/or autocrine IL-6 support of myeloid cells may further drive MDSC differentiation [64,65]. Therefore, targeting high levels of IL-6 in RCC patients might be a promising therapy.

A central finding of our study is that IL-6 levels closely correlated with lactate levels, pointing to glycolysis as a driver of myeloid IL-6 production. MCT inhibition in single-cell preparations of tumor biopsies from RCC patients and spheroid co-cultures reduced lactate efflux and re-educated tumor-associated myeloid cells toward a phenotype with lower IL-6 and higher HLA-DR but lower PD-L1 expression. Our experiments show that lactic acid alone induces only a weak IL-6 expression in monocytes but further experiments are necessary to confirm these results and to investigate the interplay with other possible factors.

scRNAseq data revealed high MCT4 expression in both tumor and myeloid cells. Experiments with pretreated spheroids indicated that tumor cells are the main functional target of MCT inhibition, consistent with reduced lactate secretion. Although myeloid cells are not highly glycolytic based on our scRNAseq data, they express MCT4 and take up lactate, which shapes their phenotype. Lactic acid incubation resulted in a strong upregulation of respiration indicating that energy metabolism is involved in the reprogramming of myeloid cells. In accordance, Tan et al. observed that glycolytic activity and MCT expression are important for an inflammatory response in macrophages [66].

Regardless of MCT4 expression and lactate uptake into myeloid cells, tumor-derived lactate could also activate MDSCs via the surface receptor GPR81 and the related mTOR/HIF1α/STAT3 pathway, although GPR81 expression is very low on human myeloid cells [22].

In vitro, lactic acid increased CD14$^+$ HLA-DR low cells and upregulated LOX-1 and S100A9, key regulators of MDSC activity [27,34]. In line, murine high-lactate tumors displayed more MDSCs and enrichment of IL-6/JAK/STAT signaling and *S100A9* expression overlapped with IL-6 receptor and IL-6/JAK/STAT signaling in human RCC scRNAseq data. As the promoter of *S100A8/9* contains potential STAT3 binding sites, the interplay between lactate and IL-6 signaling might contribute to the upregulation of *S100A9* [34], though IL-6 alone did not increase S100A9 *in vitro*. Moreover, others have shown that sodium lactate activates STAT3-related pathways in murine dendritic cellss but mainly STAT1/STAT2 pathways in macrophages, indicating that additional cell type-specific mechanisms may be involved [67]. High-lactate murine tumors also contained ROS-producing myeloid cells, aligning with reports that lactate signaling involves ROS production [68].

Lactate further promoted MDSC differentiation through HIF1α stabilization, consistent with previous reports describing hypoxia and HIF1α as a key regulator of MDSC and TAM differentiation [19,69]. Lactic acid and its sodium salt induced a CD14$^+$ HLA-DR low MDSC-like phenotype comparable to the pharmacological HIF1α stabilizer Roxadustat. In contrast, lactic acid but not Roxadustat induced LOX-1 and S100A9 expression, indicating a HIF1α-independent regulation. Lactylation of HIF1α has been shown to regulate protein stability by impairing VHL recognition and subsequent HIF1α protein degradation. Likewise, lactylation supports HIF stabilization via directly binding to the catalytic domain of prolyl hydroxylase domain-containing 2 (PHD2) in a competitive manner with α-ketoglutarate [70–73]. We also assessed global protein lactylation and observed increased lactylation upon treatment with lactic acid or sodium lactate. However, further experiments are required to clarify the link between lactylation and HIF1α stabilization in lactate-treated human monocytes.

In summary, our data suggest that tumor-derived lactate and IL-6 cooperate to promote a CD14$^+$ MDSC-like phenotype in ccRCC, contributing to an immunosuppressive tumor microenvironment and correlating with poor patient prognosis. Myeloid CD14$^+$ MDSC-like cells were consistently observed in patient tumors and reproduced in our RCC spheroid model, highlighting their functional relevance. Importantly, selective inhibition of MCTs effectively reduced lactate secretion, reprogrammed tumor-associated myeloid cells toward a less suppressive phenotype, and lowered IL-6 production, indicating that MCT targeting can modulate both tumor cells and the immunosuppressive myeloid compartment. These findings support MCT inhibition as a promising anti-metabolic strategy to counteract MDSC-mediated immune suppression and to enhance anti-tumor immunity in ccRCC.

4.1. Limitations and perspectives of our study

We propose that lactate is a key regulator of myeloid differentiation in the RCC tumor environment, possibly involving lactylation of HIF1α. Although lactate uptake, protein lactylation, and HIF1α stabilization were confirmed, specific lactylation sites and downstream pathways remain to be elucidated. The impact of MCT inhibition should also be tested with additional metabolic inhibitors such as LDH blockers.

CRediT authorship contribution statement

Nathalie Babl: Writing – review & editing, Writing – original draft, Visualization, Project administration, Investigation, Formal analysis, Conceptualization. **Florian Voll:** Visualization, Investigation, Formal analysis. **Agnieszka Martowicz:** Visualization, Validation, Software, Formal analysis, Data curation. **Christina Bruss:** Writing – original draft, Investigation, Formal analysis. **Marianna Maddaloni:** Methodology, Investigation. **Christian Schmidl:** Methodology. **Michael Rehli:** Methodology. **Stefan Loipfinger:** Software, Formal analysis. **Nicholas Strieder:** Formal analysis, Data curation. **Claudia Gebhard:** Methodology. **Petra Hoffmann:** Methodology. **Sukh M. Singh:** Writing – review & editing. **Ada Sala-Hojman:** Writing – review & editing. **Roberta Ferretti:** Writing – review & editing. **Carina Matos:** Investigation. **Malte Simon:** Visualization, Formal analysis. **Christina Brummer:** Investigation. **Annette Schnell:** Investigation. **Joshua Hofbauer:** Investigation. **Sonja-Maria Decking:** Investigation. **Peter Hau:** Methodology. **Arabel Vollmann-Zwerenz:** Methodology. **Katja Dettmer:** Methodology. **Peter J. Oefner:** Methodology. **Michael Althammer:** Investigation. **Johanna Laufs:** Investigation. **Sarah Friedl:**

Investigation. **Timo Heinrich:** Writing – review & editing, Resources. **Christian Herhaus:** Writing – review & editing, Resources. **Katja Evert:** Methodology. **Roman Mayr:** Resources. **Julieta Afonso:** Methodology. **Fatima Baltazar:** Methodology. **Wolfgang Herr:** Writing – review & editing, Resources. **Peter J. Siska:** Writing – review & editing, Resources, Project administration, Conceptualization. **Kathrin Renner:** Writing – review & editing, Supervision, Project administration, Funding acquisition, Conceptualization. **Marina Kreutz:** Writing – review & editing, Writing – original draft, Supervision, Project administration, Funding acquisition, Conceptualization.

Ethics approval

Fresh malignant tissue was surgically removed from patients with ccRCC. All subjects provided written consent according to protocols approved by the ethical committee of the University Hospital Regensburg (Nr. 16-355-101 and 08/108) in accordance with the Declaration of Helsinki.

Animal experiments were performed according to the regulations of the local government of Würzburg, Germany, and permission was obtained from the Government of Unterfranken, Germany.

MNCs were isolated from thrombocyte donation products from healthy individuals via density centrifugation. All participants provided written informed consent and the study was approved by the local ethics committee (vote numbers 13-101-0240 and 13-101-0238).

Funding

This study was supported by Merck Healthcare KGaA, Darmstadt, Germany (CrossRef Funder ID: 10.13039/100009945), the Leibniz Institute for Immunotherapy, Regensburg, Germany, the Else Kröner-Fresenius-Foundation (P.J.S.), and by the ReForM E program (IntraCom consortium) of the University Hospital Regensburg, Germany (Project No.: 3753782).

Declaration of competing interest

The authors declare the following financial interests/personal relationships which may be considered as potential competing interests: The study was supported by Merck Healthcare KGaA, Darmstadt, Germany; MCT inhibitors were provided by Merck Healthcare KGaA, Darmstadt, Germany. A.S.-H., T.H., and C.H. are employees of Merck Healthcare KGaA, Darmstadt, Germany. R.F. is an employee of EMD Serono Research & Development Institute, Inc., Billerica, MA, USA, an affiliate of Merck Healthcare KGaA, Darmstadt, Germany, Darmstadt, Germany.

Acknowledgments

We would like to express our gratitude to Alice Peuker, Gabriele Schönhammer, Marcus Kielmanowicz and Leopold Specht from the University Hospital Regensburg for their outstanding technical assistance. Furthermore, we sincerely thank Armine Matevossian from EMD Serono Research & Development Institute, Inc., Billerica, MA, USA, an affiliate of Merck KGaA, for her valuable review of the manuscript.

Sequencing of B16 tumor-infiltrating immune cells were conducted at the NGS & Data Technologies Core Unit of the Leibniz Institute of Immunotherapy (LIT), Germany (https://lit.eu/facilities/ngs-and-data-technologies). We would like to thank Hanna Stanewsky for her assistance with the single-cell RNA sequencing experiment.

We would like to thank all members of the Flow Cytometric Cell Analytics and Cell Sorting Core Facility of the LIT for their expert technical assistance with cell sorting.

We are grateful for the advice from Prof. Dr. Victor Umansky who supported the establishment of the suppression assay.

Appendix A. Supplementary data

Supplementary data to this article can be found online at https://doi.org/10.1016/j.canlet.2025.218209.

Data availability

Relevant data are available upon request from the corresponding author.

References

[1] J.J. Hsieh, M.P. Purdue, S. Signoretti, C. Swanton, L. Albiges, M. Schmidinger, et al., Renal cell carcinoma, Nat. Rev. Dis. Primers. 3 (2017) 17009.
[2] F.E. Vera-Badillo, A.J. Templeton, I. Duran, A. Ocana, P de Gouveia, P. Aneja, et al., Systemic therapy for non-clear cell renal cell carcinomas: a systematic review and meta-analysis, Eur. Urol. 67 (4) (2015) 740–749.
[3] D. Ambrosetti, M. Dufies, B. Dadone, M. Durand, D. Borchiellini, J. Amiel, et al., The two glycolytic markers GLUT1 and MCT1 correlate with tumor grade and survival in clear-cell renal cell carcinoma, PLoS One. 13 (2) (2018) e0193477.
[4] K. Singer, M. Kastenberger, E. Gottfried, C.G. Hammerschmied, M. Büttner, M. Aigner, et al., Warburg phenotype in renal cell carcinoma: high expression of glucose-transporter 1 (GLUT-1) correlates with low CD8(+) T-cell infiltration in the tumor, Int. J. Cancer. 128 (9) (2011) 2085–2095.
[5] G.L. Semenza, HIF-1: upstream and downstream of cancer metabolism, Curr. Opin. Genet. Dev. 20 (1) (2010) 51–56.
[6] S.J. Bensinger, H.R. Christofk, New aspects of the warburg effect in cancer cell biology, Semin. Cell Dev. Biol. 23 (4) (2012) 352–361.
[7] R.A. Cairns, I.S. Harris, T.W. Mak, Regulation of cancer cell metabolism, Nat. Rev. Cancer. 11 (2) (2011) 85–95.
[8] M. Gerlinger, C.R. Santos, B. Spencer-Dene, P. Martinez, D. Endesfelder, R. A. Burrell, et al., Genome-wide RNA interference analysis of renal carcinoma survival regulators identifies MCT4 as a warburg effect metabolic target, J. Pathol. 227 (2) (2012) 146–156.
[9] C.D. Bovenzi, J. Hamilton, P. Tassone, J. Johnson, D.M. Cognetti, A. Luginbuhl, et al., Prognostic indications of elevated MCT4 and CD147 across cancer types: a meta-analysis, BioMed Res. Int. 2015 (2015) 242437.
[10] Y.-W. Cao, Y. Liu, Z. Dong, L. Guo, E.-H. Kang, Y.-H. Wang, et al., Monocarboxylate transporters MCT1 and MCT4 are independent prognostic biomarkers for the survival of patients with clear cell renal cell carcinoma and those receiving therapy targeting angiogenesis, Urol. Oncol. 36 (6) (2018) 311.e15–311.e25. Available from: URL: https://pubmed.ncbi.nlm.nih.gov/29657088/.
[11] Y. Kim, J.-W. Choi, J.-H. Lee, Y.-S. Kim, Expression of lactate/H^+ symporters MCT1 and MCT4 and their chaperone CD147 predicts tumor progression in clear cell renal cell carcinoma: immunohistochemical and the cancer genome atlas data analyses, Hum. Pathol. 46 (1) (2015) 104–112.
[12] F. Xu, Y. Guan, L. Xue, S. Huang, K. Gao, Z. Yang, et al., The effect of a novel glycolysis-related gene signature on progression, prognosis and immune microenvironment of renal cell carcinoma, BMC Cancer. 20 (1) (2020) 1207.
[13] P.J. Siska, K. Singer, K. Evert, K. Renner, M. Kreutz, The immunological warburg effect: can a metabolic-tumor-stroma score (MeTS) guide cancer immunotherapy? Immunol. Rev. 295 (1) (2020) 187–202.
[14] B.I. Reinfeld, M.Z. Madden, M.M. Wolf, A. Chytil, J.E. Bader, A.R. Patterson, et al., Cell-programmed nutrient partitioning in the tumour microenvironment, Nature 593 (7858) (2021) 282–288.
[15] C.L. Markert, J.B. Shaklee, G.S. Whitt, Evolution of a gene. Multiple genes for LDH isozymes provide a model of the evolution of gene structure, function and regulation, Science. 189 (4197) (1975) 102–114.
[16] P. Seth, E. Csizmadia, A. Hedblom, M. Vuerich, H. Xie, M. Li, et al., Deletion of lactate Dehydrogenase-A in myeloid cells triggers antitumor immunity, Cancer Res. 77 (13) (2017) 3632–3643.
[17] A.-C. Frank, R. Raue, D.C. Fuhrmann, E. Sirait-Fischer, C. Reuse, A. Weigert, et al., Lactate dehydrogenase B regulates macrophage metabolism in the tumor microenvironment, Theranostics. 11 (15) (2021) 7570–7588.
[18] O.R. Colegio, Lactic acid polarizes macrophages to a tumor-promoting state, OncoImmunol. 5 (3) (2016) e1014774.
[19] O.R. Colegio, N.-Q. Chu, A.L. Szabo, T. Chu, A.M. Rhebergen, V. Jairam, et al., Functional polarization of tumour-associated macrophages by tumour-derived lactic acid, Nature. 513 (7519) (2014) 559–563.
[20] R. Sangsuwan, B. Thuamsang, N. Pacifici, R. Allen, H. Han, S. Miakicheva, et al., Lactate exposure promotes immunosuppressive phenotypes in innate immune cells, Cell. Mol. Bioeng. 13 (5) (2020) 541–557.
[21] S.C. Stone, R.A.M. Rossetti, K.L.F. Alvarez, J.P. Carvalho, P.F.R. Margarido, E. C. Baracat, et al., Lactate secreted by cervical cancer cells modulates macrophage phenotype, J. Leukoc. Biol. 105 (5) (2019) 1041–1054.
[22] X. Yang, Y. Lu, J. Hang, J. Zhang, T. Zhang, Y. Huo, et al., Lactate-modulated immunosuppression of myeloid-derived suppressor cells contributes to the radioresistance of pancreatic cancer, Cancer Immunol. Res. 8 (11) (2020) 1440–1451.
[23] Z. Husain, Y. Huang, P. Seth, V.P. Sukhatme, Tumor-derived lactate modifies antitumor immune response: effect on myeloid-derived suppressor cells and NK cells, J. Immunol. 191 (3) (2013) 1486–1495.

[24] J. He, X. Chai, Q. Zhang, Y. Wang, Y. Wang, X. Yang, et al., The lactate receptor HCAR1 drives the recruitment of immunosuppressive PMN-MDSCs in colorectal cancer, Nat. Immunol. 26 (3) (2025) 391–403.
[25] W. Li, T. Tanikawa, I. Kryczek, H. Xia, G. Li, K. Wu, et al., Aerobic glycolysis controls myeloid-derived suppressor cells and tumor immunity via a specific CEBPB isoform in triple-negative breast cancer, Cell Metab. 28 (1) (2018) 87–103. e6.
[26] Y.G. Najjar, P. Rayman, X. Jia, P.G. Pavicic, B.I. Rini, C. Tannenbaum, et al., Myeloid-derived suppressor cell subset accumulation in renal cell carcinoma parenchyma is associated with intratumoral expression of IL1β, IL8, CXCL5, and Mip-1α, Clin. Cancer Res. 23 (9) (2017) 2346–2355.
[27] T. Condamine, G.A. Dominguez, J.-I. Youn, A.V. Kossenkov, S. Mony, K. Alicea-Torres, et al., Lectin-type oxidized LDL receptor-1 distinguishes population of human polymorphonuclear myeloid-derived suppressor cells in cancer patients, Sci. Immunol. 1 (2) (2016).
[28] O.V. Kovaleva, D.V. Samoilova, M.S. Shitova, A. Gratchev, Tumor associated macrophages in kidney cancer, Anal. Cell. Pathol. 2016 (2016) 9307549.
[29] S. Chen, S. Qian, L. Zhang, X. Pan, F. Qu, Y. Yu, et al., Tumor-associated macrophages promote migration and invasion via modulating IL-6/STAT3 signaling in renal cell carcinoma, Int. Immunopharmacol. 111 (2022) 109139.
[30] G. Gudbrandsdottir, H.H. Aarstad, L. Bostad, K.M. Hjelle, H.J. Aarstad, Ø. Bruserud, et al., Serum levels of the IL-6 family of cytokines predict prognosis in renal cell carcinoma (RCC), Cancer Immunol. Immunother. 70 (1) (2021) 19–30.
[31] M. Pilskog, G.H. Nilsen, C. Beisland, O. Straume, Elevated plasma interleukin 6 predicts poor response in patients treated with sunitinib for metastatic clear cell renal cell carcinoma, Cancer Treatment. Res. Commun. 19 (2019) 100127.
[32] Y. Wang, Y. Zhang, Prognostic role of interleukin-6 in renal cell carcinoma: a meta-analysis, Clin. Transl. Oncol. 22 (6) (2020) 835–843.
[33] Q. Fu, Y. Chang, H. An, H. Fu, Y. Zhu, Le Xu, et al., Prognostic value of interleukin-6 and interleukin-6 receptor in organ-confined clear-cell renal cell carcinoma: a 5-year conditional cancer-specific survival analysis, Br. J. Cancer 113 (11) (2015) 1581–1589.
[34] P. Cheng, C.A. Corzo, N. Luetteke, B. Yu, S. Nagaraj, M.M. Bui, et al., Inhibition of dendritic cell differentiation and accumulation of myeloid-derived suppressor cells in cancer is regulated by S100A9 protein, J. Exp. Med. 205 (10) (2008) 2235–2249.
[35] H. Tsukamoto, K. Fujieda, M. Hirayama, T. Ikeda, A. Yuno, K. Matsumura, et al., Soluble IL6R expressed by myeloid cells reduces tumor-specific Th1 differentiation and drives tumor progression, Cancer Res. 77 (9) (2017) 2279–2291.
[36] H. Tsukamoto, K. Fujieda, S. Senju, T. Ikeda, H. Oshiumi, Y. Nishimura, Immune-suppressive effects of interleukin-6 on T-cell-mediated anti-tumor immunity, Cancer Sci. 109 (3) (2018) 523–530.
[37] H. Liu, J. Shen, K. Lu, IL-6 and PD-L1 blockade combination inhibits hepatocellular carcinoma cancer development in mouse model, Biochem. Biophys. Res. Commun. 486 (2) (2017) 239–244.
[38] T.A. Mace, R. Shakya, J.R. Pitarresi, B. Swanson, C.W. McQuinn, S. Loftus, et al., IL-6 and PD-L1 antibody blockade combination therapy reduces tumour progression in murine models of pancreatic cancer, Gut 67 (2) (2018) 320–332.
[39] Y. Ohno, Y. Toyoshima, H. Yurino, N. Monma, H. Xiang, K. Sumida, et al., Lack of interleukin-6 in the tumor microenvironment augments type-1 immunity and increases the efficacy of cancer immunotherapy, Cancer Sci. 108 (10) (2017) 1959–1966.
[40] T. Stuart, A. Butler, P. Hoffman, C. Hafemeister, E. Papalexi, W.M. Mauck, et al., Comprehensive integration of single-cell data, Cell 177 (7) (2019) 1888–1902.e21.
[41] G. Yu, L.-G. Wang, Y. Han, Q.-Y. He, clusterProfiler: an R package for comparing biological themes among gene clusters, OMICS 16 (5) (2012) 284–287.
[42] R. Li, J.R. Ferdinand, K.W. Loudon, G.S. Bowyer, S. Laidlaw, F. Muyas, et al., Mapping single-cell transcriptomes in the intra-tumoral and associated territories of kidney cancer, Cancer Cell 40 (12) (2022) 1583–1599.e10.
[43] T. Mitchell, Ruoyan Li, Mapping Single Cell Transcriptomes in Kidney Cancer, Mendeley Data, V1, 2022, https://doi.org/10.17632/g67bkbnhhg.1.
[44] C. Xu, R. Lopez, E. Mehlman, J. Regier, M.I. Jordan, N. Yosef, Probabilistic harmonization and annotation of single-cell transcriptomics data with deep generative models, Mol. Syst. Biol. 17 (1) (2021) e9620.
[45] A. Gayoso, R. Lopez, G. Xing, P. Boyeau, V. Valiollah Pour Amiri, J. Hong, et al., A python library for probabilistic analysis of single-cell omics data, Nat. Biotechnol. 40 (2) (2022) 163–166.
[46] M.D. Young, T.J. Mitchell, F.A. Vieira Braga, M.G.B. Tran, B.J. Stewart, J. R. Ferdinand, et al., Single-cell transcriptomes from human kidneys reveal the cellular identity of renal tumors, Science. 361 (6402) (2018) 594–599.
[47] M. Ždralević, A. Brand, L. Di Ianni, K. Dettmer, J. Reinders, K. Singer, et al., Double genetic disruption of lactate dehydrogenases A and B is required to ablate the "Warburg effect" restricting tumor growth to oxidative metabolism, J. Biol. Chem. 293 (41) (2018) 15947–15961.
[48] N. Babl, S.-M. Decking, F. Voll, M. Althammer, A. Sala-Hojman, R. Ferretti, et al., MCT4 blockade increases the efficacy of immune checkpoint blockade, J. Immunother. Cancer 11 (10) (2023).
[49] P. Heinrich, C. Kohler, L. Ellmann, P. Kuerner, R. Spang, P.J. Oefner, et al., Correcting for natural isotope abundance and tracer impurity in MS-, MS/MS- and high-resolution-multiple-tracer-data from stable isotope labeling experiments with IsoCorrectoR, Sci. Rep. 8 (1) (2018) 17910.
[50] G. Kroemer, J. Pouyssegur, Tumor cell metabolism: cancer's achilles' heel, Cancer Cell. 13 (6) (2008) 472–482.
[51] V. Bronte, S. Brandau, S.-H. Chen, M.P. Colombo, A.B. Frey, T.F. Greten, et al., Recommendations for myeloid-derived suppressor cell nomenclature and characterization standards, Nat. Commun. 7 (2016) 12150.
[52] E. Gottfried, L.A. Kunz-Schughart, R. Andreesen, M. Kreutz, Brave little world: spheroids as an in vitro model to study tumor-immune-cell interactions, Cell Cycle 5 (7) (2006) 691–695.
[53] K. Renner, C. Bruss, A. Schnell, G. Koehl, H.M. Becker, M. Fante, et al., Restricting glycolysis preserves T cell effector functions and augments checkpoint therapy, Cell Rep. 29 (1) (2019) 135–150.e9.
[54] J. Galon, A. Costes, F. Sanchez-Cabo, A. Kirilovsky, B. Mlecnik, C. Lagorce-Pagès, et al., Type, density, and location of immune cells within human colorectal tumors predict clinical outcome, Science. 313 (5795) (2006) 1960–1964.
[55] M.J.M. Gooden, GH de Bock, N. Leffers, T. Daemen, H.W. Nijman, The prognostic influence of tumour-infiltrating lymphocytes in cancer: a systematic review with meta-analysis, Br. J. Cancer 105 (1) (2011) 93–103.
[56] R.H. Thompson, H. Dong, C.M. Lohse, B.C. Leibovich, M.L. Blute, J.C. Cheville, et al., PD-1 is expressed by tumor-infiltrating immune cells and is associated with poor outcome for patients with renal cell carcinoma, Clin. Cancer Res. 13 (6) (2007) 1757–1761.
[57] W.S. Webster, C.M. Lohse, R.H. Thompson, H. Dong, X. Frigola, D.L. Dicks, et al., Mononuclear cell infiltration in clear-cell renal cell carcinoma independently predicts patient survival, Cancer 107 (1) (2006) 46–53.
[58] A. Brand, K. Singer, G.E. Koehl, M. Kolitzus, G. Schoenhammer, A. Thiel, et al., LDHA-associated lactic acid production blunts tumor immunosurveillance by T and NK cells, Cell Metab. 24 (5) (2016) 657–671.
[59] P. Fisel, S. Kruck, S. Winter, J. Bedke, J. Hennenlotter, A.T. Nies, et al., DNA methylation of the SLC16A3 promoter regulates expression of the human lactate transporter MCT4 in renal cancer with consequences for clinical outcome, Clin. Cancer Res. 19 (18) (2013) 5170–5181.
[60] V. Umansky, C. Blattner, C. Gebhardt, J. Utikal, The role of myeloid-derived suppressor cells (MDSC) in cancer progression, Vaccines (Basel) 4 (4) (2016).
[61] P.E. Oberstein, A. Dias Costa, E.A. Kawaler, V. Cardot-Ruffino, O.E. Rahma, N. Beri, et al., Blockade of IL1β and PD1 with combination chemotherapy reduces systemic myeloid suppression in metastatic pancreatic cancer with heterogeneous effects in the tumor, Cancer Immunol. Res. 12 (9) (2024) 1221–1235.
[62] M.P. Gustafson, Y. Lin, J.S. Bleeker, D. Warad, M.K. Tollefson, P.L. Crispen, et al., Intratumoral CD14+ cells and circulating CD14+HLA-DRlo/neg monocytes correlate with decreased survival in patients with clear cell renal cell carcinoma, Clin. Cancer Res. 21 (18) (2015) 4224–4233.
[63] H. Toge, T. Inagaki, Y. Kojimoto, T. Shinka, I. Hara, Angiogenesis in renal cell carcinoma: the role of tumor-associated macrophages, Int. J. Urol. 16 (10) (2009) 801–807.
[64] R. Weber, C. Groth, S. Lasser, I. Arkhypov, V. Petrova, P. Altevogt, et al., IL-6 as a major regulator of MDSC activity and possible target for cancer immunotherapy, Cell. Immunol. 359 (2021) 104254.
[65] R. Weber, Z. Riester, L. Hüser, C. Sticht, A. Siebenmorgen, C. Groth, et al., IL-6 regulates CCR5 expression and immunosuppressive capacity of MDSC in Murine melanoma, J. Immunother. Cancer 8 (2) (2020).
[66] Z. Tan, N. Xie, S. Banerjee, H. Cui, M. Fu, V.J. Thannickal, et al., The monocarboxylate transporter 4 is required for glycolytic reprogramming and inflammatory response in macrophages, J. Biol. Chem. 290 (1) (2015) 46–55.
[67] R. Sangsuwan, B. Thuamsang, N. Pacifici, P. Tachachartvanich, D. Murphy, A. Ram, et al., Identification of signaling networks associated with lactate modulation of macrophages and dendritic cells, Heliyon 11 (3) (2025) e42098.
[68] T. Hashimoto, R. Hussien, S. Oommen, K. Gohil, G.A. Brooks, Lactate sensitive transcription factor network in L6 cells: activation of MCT1 and mitochondrial biogenesis, FASEB J. : official publication of the Federation of American Societies for Experimental Biology 21 (10) (2007) 2602–2612.
[69] C.A. Corzo, T. Condamine, L. Lu, M.J. Cotter, J.-I. Youn, P. Cheng, et al., HIF-1α regulates function and differentiation of myeloid-derived suppressor cells in the tumor microenvironment, J. Exp. Med. 207 (11) (2010) 2439–2453.
[70] X. Wang, J. Huang, W. Fan, N. Li, H. Yang, W. Yang, et al., Lactate-binding protein DNMT3A in HRMECs promotes angiogenesis by upregulating VEGFA through HIF-1α lactylation, Genome Biol. 26 (1) (2025) 377.
[71] C. Li, C. Fu, W. Zhou, H. Li, Z. Liu, G. Wu, et al., Lactylation modification of HIF-1α enhances its stability by blocking VHL recognition, Cell Commun. Signal. 23 (1) (2025) 364.
[72] X.H. Hui, T. Feng, Adipocyte-derived lactate potentiates obesity-evoked adipose macrophage inflammation, J Endocr Soc 5 (Supplement_1) (2021) A40–A41.
[73] J. Gao, R. Liu, K. Huang, Z. Li, X. Sheng, K. Chakraborty, et al., Dynamic investigation of hypoxia-induced L-lactylation, Proc. Natl. Acad. Sci. 122 (10) (2025) e2404899122.